NON-THERMAL RADIO EMISSION FROM DARK MATTER ANNIHILATION PROCESSES IN SIMULATED COMA LIKE GALAXY CLUSTERS

By

Fitsum W/Gerima Beyene

A THESIS PRESENTED TO

THE PROGRAM OF GRADUATE STUDIES
ADDIS ABABA UNIVERSITY

IN PARTIAL FULFILLMENT OF THE REQUIREMENTS
FOR THE DEGREE

MASTER OF SCIENCE in PHYSICS

(ASTRONOMY and ASTROPHYSICS)

ADDIS ABABA, ETHIOPIA

JULY 2018

ADDIS ABABA UNIVERSITY

PROGRAM OF GRADUATE STUDIES

NON-THERMAL RADIO EMISSION FROM DARK MATTER ANNIHILATION PROCESSES IN SIMULATED COMA LIKE GALAXY CLUSTERS

By

Fitsum W/Gerima Beyene

Department of Physics

Addis Ababa University

Approved by the Examining Board:

Dr. Remudin Reshid Signature _____
Advisor

Dr. Mirjana Povic Signature _____
Examiner

Dr. Getinet Felek Signature _____
Examiner

Dated: July 2018

ADDIS ABABA UNIVERSITY

Date: **July 2018**

Author: **Fitsum W/Gerima Beyene**

Title: **Non-Thermal Radio Emission from Dark Matter Annihilation Processes in Simulated Coma like Galaxy Clusters**

Department: **Department of Physics**

Degree: **M.Sc.** Convocation: **July** Year: **2018**

Permission is herewith granted to Addis Ababa University to circulate and to have copied for non-commercial purposes, at its discretion, the above title upon the request of individuals or institutions.

_____

Signature of Author

This Work is Dedicated

to

My Father

WOLDEGERIMA BEYENE

Table of Contents

List of Tables

List of Figures

Acknowledgements

First of all I would like to thank my Father God, whose creation I will pursue through the mathematical and physical laws of the Universe.

Secondly, I am grateful to my advisor Dr. Remudin Reshid for the guidance, heartful support and direction he offered to us and for all the resources he made avialable as we carryout this thesis work.

I would like to express my appreciation to the department of physics and to all our instructors for the conducive enviroment they have created for us as we make this study, and my special thanks goes to Dr. Belayneh Mesfin for his kindness and beautiful lecture on tensor calculus.

The priceless comments and suggestions I obtained from Dr. Mirjana Povic, which have strengthened this work, are very appreciated.

The support I obtained from Fikre (a statistical physics Phd student) in installing computer programs like ubuntu and Abdu Seid my classmate on the thesis writing techqunics through Texmaker is all unforgettable, so I thank them both.

I also would like to appreciate all my classmates for the memoriable events we have spent in this two years of our study.

Last but not list, I would like to thank my family especially my father who always motivate and strengthen me to focus on my studies and my sister Lemlem (Lemi) for all her support and blessing words.

Addis Ababa University Fitsum W/Gerima Beyene

July, 2018

Abbreviations

DM	**D**ark **M**atter
WIMP	**W**eakly **I**nteracting **M**assive **P**article
MACHO	**MA**ssive **C**ompact **H**alo **O**bjects
SGC280	**S**imulated **G**alaxy **C**luster **280**
SGC282	**S**imulated **G**alaxy **C**luster **282**
ICM	**I**nter-**C**luster **M**edium
SM	**S**tandard **M**odel
MUSIC	**MU**ltiDark **SI**mulations of galaxy **C**lusters
ICS	**I**nverse **C**ompton **S**cattering
SPH	**S**mooth **P**article **H**ydrodynamics

Physical Constants

Speed of Light	$c = 2.997\ 924\ 58 \times 10^{8}$ m s^{-1}
Mass of an Electron	$m_e = 9.11 \times 10^{-28}$ g
Mass of a Proton	$m_p = 1.67 \times 10^{-24}$ g
Gravitational Constant	$G = 6.673 \times 10^{-11}$ Nm^2/kg^2
Mass of the Sun	$M_\odot = 1.99 \times 10^{33}$ g
Classical radius of an Electron	$r_e = 2.82 \times 10^{-13}$ cm
Boltzmann Constant	$k = 1.3806505 \times 10^{-23}$ J K^{-1}
Hubble Constant	$H_0 = 100h$ kms^{-1} Mpc^{-1}
Dimensionless parameter	$h = 0.6727 \pm 0.0066$

Unit Conversion

Jansky	Jy = 10^{20} Gev cm^{-2} s^{-1} Hz^{-1}
Kiloparsec	kpc = $3.08568025 \times 10^{21}$ cm
Mega electron volt	Mev = 1.78×10^{-27} g
Solar mass	$M_{\odot}$ = 1.99×10^{33} g
Solar mass per kiloparsec cube	$M_{\odot}/kpc^3$ = 6.7733×10^{-32} g/cm^3

Abstract

Taking secondary particles produced from dark matter annihilation process to the origin of the extended diffuse radio emissions observed in galaxy clusters, we studied both their morphology and radio spectral profile using simulated Coma like galaxy clusters. We have considered a neutralino annihilation channel dominated by $b\bar{b}$ species with a branching ratio of 1 and neutralino mass of 35 GeV with annihilation cross-section times velocity value of 1×10^{-26} cm^3 s^{-1}. The radio emission maps produced for the two simulated galaxy clusters which are based on the MUsic SImulation of galaxy Clusters (MUSIC)-dataset reveal the observed radio halo morphology showing radio emissions both from the central regions of the cluster and substructures lying off-center. The flux density curve is in a good agreement for $\nu \leq 2$ GHz with the obsevational values of (Thierbach et al., 2003) for the Coma cluster of galaxies showing a small deviation at higher frequencies. The small spectral index fluctuations observed in the wide cluster regions corresponds to the DM substructures scattered with in the clusters. The spectral index values $\sim$ (-0.8, -1.0) and $\sim$ (-1.6, -2.2) obtained in the very center and dark matter substructure (cluster periphery) are in a good agreement with the work of (Giovannini et al., 1993). The central spectral flattening and the peripheral steepening explain the dense central and underdense peripheral DM regions, respectively.

Introduction

A revolution in the understanding of the Universe happened when Edwin Hubble measured the distance of the Andromeda Galaxy providing evidence that our galaxy is among many more galaxies in the Universe (Roos, 2015). From the rate of expansion of the Universe we now know that it began roughly 14 billion years ago in the hot and dense state of the "Hot Big Bang" and it has become evident that the Universe is comprised of some extremely interesting structures such as galaxies, clusters, superclusters, voids and great walls (Hawley and Holcomb, 2005). The attractive force of gravity gave rise to all structures we observe today. Observations based on supernovae measurements now give indications that the Universe is not only expanding but also its rate is accelerating. Cosmology enters a precision era when the cosmic microwave background (CMB) is mapped with high accuracy by WMAP. As a result of which the curvature and matter budget of the Universe were able to be determined very accurately (Basu et al., 2010). Now it is known that the Universe is composed of 4.9% the ordinary baryonic matter, which is the usual form of matter in diffuse gas, stars and galaxies, 26.8% by dark matter (DM) and the remaining 68.3% is dark energy (Ade et al., 2016). According to cosmological models the fate of our Universe lies on the amount of DM and dark energy present. If the DM dominates over dark energy the Universe will collapse and end up in a singularity but if the dark energy dominates it will expand infinitly. So it is very crucial to know the nature of this invisible realm of our Universe.

DM is believed to be the responsible agent for the formation of galaxies and galaxy clusters, through its gravitational attraction it brought them into a gravitationally bounded structures (**?**). For this reason both galaxies and clusters of galaxies are expected to be dominated by DM. A typical cluster of galaxies may have masses about 10^{15} $M_{\odot}$, and volumes of about 100 Mpc^3 with DM upto $\sim 80\%$, some of the luminous matter is in galaxies (3 - 5%) and the rest is in diffuse hot gas (15 - 17%) (Feretti et al., 2012). Galaxy clusters are of great importance as they trace

the most pronounced density peaks of large-scale structure that are localized close to their ongoing formation. They manifest the cosmological structure formation and DM in the Universe. Numerical simulations show that galaxy clusters form through grouping of smaller objects or "accretion" of clumps along the filaments and rarely through "mergers" with larger clusters which is also known as "bottom-up" scenario. The largest clusters often form at the intersection of the filamentary structures (Ryu et al., 2003). The formation of these structures is driven by DM (Kolb and Turner, 1990).

Observations are revealing that there is a diffuse radio emission in clusters of galaxies which is non-thermal synchrotron in origin. The diffuse, extended radio emission of the Coma cluster of galaxies was detected by Large et al. (1959) and first investigated by Willson (1970). Several years later, extended diffuse emission was also detected at the periphery of the Coma cluster and at the center of the Perseus cluster (Vacca et al., 2014). This diffuse extended radio sources, are not associated to the individual galaxies and their origin and evolution is still a matter of debate. Several suggestions for the mechanism of transferring energy into the relativistic electron population and for the origin of relativistic electrons themselves have been made: reacceleration of relativistic electrons due to the turbulence and shock waves from cluster mergers suggested by primary elecron model, secondary electrons resulting from hadronic collisions of relativistic protons with the ICM gas protons (see e.g. Brunetti et al. (2001)) as suggested by the secondary electron model, and DM annihilation/decay processes in galaxy clusters. It is therefore important to carry out new researches aimed at discriminating between these theoretical models.

Motivation and Objectives

Motivated by this observations in this work we study the radio emission from DM annihilation/decay processes in two simulated Coma like galaxy clusters at seven different frequencies choosen to make comparision with the observational results. We intend to model the radio emission from DM annihilation processes because of the fact that the clusters are domonated by DM and since Coma cluster is the best studied we choose simulated Coma like galaxy clusters. For this purpose we took two simulated Coma like galaxy clusters (SGC280 and SGC282) from the MUSIC-dataset (see section 3.2). Among large number of proposed particle

candidates for DM, we have considered the most favored one which is Weakly Interacting Massive Particles (WIMPs). WIMPs have several important particle properties such as mass, stability, scattering cross-section with nucleons, and cross-section for pair annihilation etc., which are both theoretically well motivated and constrained through various experiments as has been discussed widely in **?**. There are basically three different strategies to find out how WIMPs migth be detected. These are direct detection mechanism through WIMP scattering off nuclei, an indirect detection through the observation of emission from the DM annihilation/decay process, and detection at the colliders through the search for annihilation by-products (Lisanti, 2017). Now it is clear that our work has two sides: On one hand, we are searching for source of this realtivistic electrons which are responsible for the diffused radio emission and on the other hand we are making an indirect detection of DM within the galaxy clusters.

With this in mind, our specific objectives in making this study are: to produce radio emission maps at different frequencies, to make a flux density curve and study the integrated radio spectrum, and lastly to study the spatial variation of spectral index values. In addition, we will make an overview of the DM distribution using the density maps of the two clusters.

This thesis is organized in the following manner: we first present, in chapter one, a simple introduction to cosmology, cosmological principles and models of the Universe. Then we focus on the observational evidences of DM in galaxies and galaxy clusters through the study of rotational curves and gravitational lensing. We close chapter one answering questions such as: what is the identity of DM and how it could be detected. In chapter two the diffused radio emission from galaxy clusters and different models for the possible sources of the relativistic electrons which are responsible for the diffused radio emission are broadly discussed. Where as in chapter three we present the modeling for the radio emission with the proper mathematical formulation of the magnetic field strength, the "electron equilibrium spectra", the local emissivity and ultimately the flux. We conclude chapter three by introducing our data sources and the simulation techniques followed to analyse our data. In chapter four the results (maps and graphs) obtained from the simulation and their elaborate discussions are presented. Finally, we gave conclusion of our work in chapter five.

CHAPTER 1

Cosmology and the theory of dark matter

1.1 Introduction

Stars, galaxies, interstellar and intergalactic matter, radiation, magnetic field and cosmic rays are all the contents of the Universe. The question then naturally arises: What is the physical and kinematical nature of the Universe itself, when considered in its entirety? Cosmology is the science which attempts to give a satisfactory answer to this fundamental question regarding the understanding of the phenomena behind the cosmos (Basu et al., 2010). It is the study of the origin, content, form, and time evolution of the Universe (Serway et al., 2004). Cosmology aims to explain the origin and evolution of the entire contents of the Universe, the underlying physical processes, and there by to obtain a deeper understanding of the laws of physics assumed to hold throughout the Universe (Roos, 2015).

The basic requirement in formulating a theory of cosmology lies in truly knowing some of the basic facts about the Universe. These are, the shape (geometry) and size, the mass density and the total mass content, the age, the phase of its present dynamical behaviour, and its chemical evolution with time. All this informations are very fundamental for the understanding of the nature of any object. For any individual object or group of objects occupying any local region of space, these informations are not very difficult to acquire through experiments and theoretical postulates. But for the Universe as a whole, it is precisely these simple facts which pose great diffucalties to be known. In fact, none of these basic facts has yet been known with any amount of definiteness when the Universe as a whole is concerned. Even the most powerful optical and radio telescopes available at present are unable to fathom the whole depth of the Universe. And whatever observations at large distances have been obtained, their true interpretation have very often eluded the scientists (Basu et al., 2010).

We have dedicted this chapter to one of the profound branches of Astrophysics, i.e. Cosmology and the mystreous form of matter, i.e. dark matter (DM). In the first two sections we introduce the cosmological principles and models of our Universe. Where as the rest sections opens a way to DM through its observational evidences, present the possible cadidates and then indicate the detection mechanisms.

1.2 The cosmological principle of the Universe

Whenever science enters a new field and is faced with a dearth of observational or experimental data some guiding principle is usually needed to assist during the first tentative steps towards a theoretical understanding. Therefore, in this section the guiding principle on which all the cosmological theories and predictions are based will be discussed.

The Cosmological Principle is the assertion that, on sufficiently large scales, the Universe is both homogeneous and isotropic. Homogeneity is the property of being identical everywhere in space, while isotropy is the property of looking the same in every direction (Coles and Lucchin, 2003). The main contention of this principle is that the Universe presents the same picture at any particular epoch in whichever direction we may look from whatever position, except for local irregularities which are of statistical nature. Observations do really tend to confirm that the large-scale aspect of the Universe is isotropic and homogeneous. It is now revealed that no matter which direction of the Universe we look to, the type and number density of galaxies are essentially the same. Of course the colours of galaxies become increasingly redder as we look to greater distances on account of increasing redshifts, but this change in colours is not at all dependent on directions. In whichever direction we may look at, the law of redshifts remains the same. Thus the observable aspects of the Universe are found to maintain complete independence with respect to directions. In other words, the Universe is isotropic. No direction is prefered so far as observable aspects of the Universe are concerned. Let us consider the case of the homogeneity of the Universe. This means that the picture of the Universe that we observe locally doesnot differ from the picture at large distance. In other words, the conditions and the enviroments are independent of the locality of the Universe. Of course, we must remember that the redshift of objects are different at different distances. But what we like to emphasize is that in the absence of the effects of recessional velocities that cause redshifts,

the distant parts of the Universe would not have been different from our local enviroment. This observational aspects underlies the basic postulate that the Universe is homogeneous. The cosmological principle with larger field of application asserts that the physical laws which are valid locally, are also valid in any arbitrary region of the Universe (Basu et al., 2010).

1.3 Cosmological models of the Universe

To "build" a cosmological model, in a modern sense, three fundamental ingredients are needed: *Einstein's equation*, relating the geometry of the Universe with its matter and energy content. *Metrics*, describing the symmetries of the problem. *Equation of state*, specifying the physical properties of the matter and energy content.

The Einstein's equation is given as

$$\mathbf{R}_{\mu\nu} - \frac{1}{2} g_{\mu\nu} \mathbf{R} = -\frac{8\pi G}{c^4} T_{\mu\nu} + \Lambda g_{\mu\nu}, \tag{1.1}$$

where $\mathbf{R}_{\mu\nu}$ and $\mathbf{R}$ are the Ricci tensor and scalar, respectively, $g_{\mu\nu}$ is the metric tensor, G in gravitational constant, $T_{\mu\nu}$ is the energy-momentum tensor, and Λ is called the cosmological constant.

To solve this equation one has to specify the symmetries of the problem. Usually one assumes the properties of statistical homogeneity and isotropy of the Universe, which greatly simplifies the mathematical analysis.

The properties of isotropy and homogeneity imply a specific form of the metric: the line element can in fact be expressed as

$$ds^2 = -c^2 dt^2 + R^2(t) \left(\frac{dr^2}{1 - kr^2} + r^2 d\Omega^2 \right), \tag{1.2}$$

where R(t) is called scale factor, $d\Omega^2 = d\phi^2 + \sin^2\theta d\theta^2$ and the constant k, describing the spatial curvature, can take the values k = -1, 0, +1 (r, θ and ϕ are coordinates in the spherical system).

The Einstein's equation can be solved with this metric, one of its components leading to the Friedmann equation

$$\left(\frac{\dot{R}}{R}\right)^2 + \frac{k}{R^2} = \frac{8\pi G}{3}\rho_{tot}, \tag{1.3}$$

here ρ_{tot} is the total average energy density of the Universe.

The Hubble parameter which determines the rate of expansion of the Universe is introduced as

$$H(t) = \frac{\dot{R}(t)}{R(t)} \tag{1.4}$$

A recent estimate of the present value of the Hubble parameter, H_O (also referred to as the Hubble constant), expressed interms of the dimensionless factor h is

$$H_O = 100h\ kms^{-1}\ Mpc^{-1},$$

h = 0.6727 $\pm$ 0.0066 based on the Planck data (Ade et al., 2016). We see from Eq1.3 that the Universe is flat (k = 0) when the energy density equals the critical density, ρ_c :

$$\rho_c = \frac{3H^2}{8\pi G} \tag{1.5}$$

The abundance of a substance in the Universe (matter, radiation or vacuum energy) is frequently expressed in units of ρ_c. We thus define the quantity Ω_i as the density parameter of a substance of species i and density ρ_i as

$$\Omega_i = \frac{\rho_i}{\rho_c} \tag{1.6}$$

It is also customary to define

$$\Omega = \sum_i \Omega_i = \sum_i \frac{\rho_i}{\rho_c} \tag{1.7}$$

in terms of which the Friedmann equation Eq1.3 can be written

$$\Omega - 1 = \frac{k}{H^2R^2} \tag{1.8}$$

The sign of k is therefore determined by whether Ω is greater than, equal to, or less than one (see Tab. 1.1) describing closed, flat and open Universe respectively.

$\rho < \rho_c$	$\Omega < 1$	$k = -1$	open
$\rho = \rho_c$	$\Omega = 1$	$k = 0$	flat
$\rho > \rho_c$	$\Omega > 1$	$k = 1$	closed

Table 1.1: Classification of cosmological models based on the value of the average density, ρ, in terms of the critical density, ρ_c (Bertone et al.).

Depending on the matter content of our Universe (for the matter and energy budget of the Universe see Fig. 1.2), energy arguments enable us to predict how our Universe ends and the future behavior of the models corresponding to each of these geometries: the flat (k = 0) and hyperbolic (k = -1) models will expand forever, while the spherical model (k = +1) will recollapse into something conventionally called the big crunch. The spherical model both begins and ends with a bang; it recollapses back to R = 0 (see Fig. 1.1). The flat and hyperbolic models, by virtue of their endless expansion, end not with a bang, but a whimper (Hawley and Holcomb, 2005).

According to the "Hot Big Bang" model the whole Universe was once in the form of

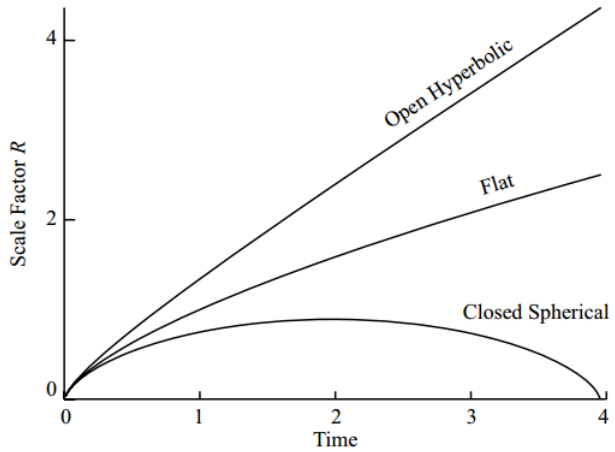

Figure 1.1: The behavior of the scale factor for the three different geometries of the standard models. All begin with a big bang. The k = +1 spherical universe expands to a maximum size, then contracts to a big crunch. While both flat (k = 0) and hyperbolic (k = -1) Universes expand forever, the hyperbolic Universe expands at a faster rate than does the flat Universe (Hawley and Holcomb, 2005).

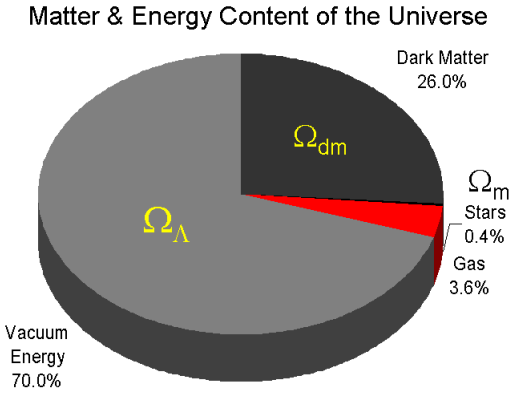

Figure 1.2: The matter energy budget of the Universe (Kolb and Turner, 1990)

a singularity, this being an extremely hot and dense state which evolve into a cool and tenuous state as a result of expansion that is still going on today.

The Hot Big Bang cosmology is an impressive framework within which cosmologists are able to interpret the many kinds of observations they are now able to make. Five pieces of strong evidence in its favour stand out: the expansion of the Universe, the predicted age of the Universe, the existence and thermal form of the cosmic microwave background, the relative abundances of the light elements predicted by cosmic nucleosynthesis, and the ability to predict the observed structures in the galaxy distribution and cosmic microwave background (Hawley and Holcomb, 2005).

1.4 Dark matter in galaxy and galaxy clusters

1.4.1 Introduction to galaxy clusters

Galaxies are gravitationally bound systems which comprises of stars, interstellar medium, stellar reminants and DM. A group of galaxies forms a galaxy cluster which is the largest gravitationally bounded system in our Universe and is composed of galaxies, intergalactic medium and DM. The larger clusters are richer and more compact aggregates of galaxies. As early as 1933, Harlow Shapley catalogued 25 clusters. Many more were discovered in the subsequent years by F. Zwicky and his collaborators and by G. Abell (Abell et al., 1989). Zwicky proposed his famous model of distribution of galaxies, that all galaxies belong to clusters. Zwicky's catalogue of galaxies lists several thousand clusters.

Analysis of the shape and structure (morphology) of clusters has led to the idea that they can broadly be divided into two categories: irregular and regular (Dressler, 1980). Their structures differ principally in two respects, namely, their sphericity in shape and central concentration. The irregular clusters possess no well defined regular shape and present more or less amorphous appearance. They are much more common in space than the regular ones. The number of galaxies in irregular clusters range from a few to as many as several thousands. Examples of rich irregular clusters are Virgo and Hercules (Basu et al., 2010). The regular clusters of galaxies are much rarer objects compared to the irregular clusters. They have more or less spherical symmetry and possess great central concentration. Rich regular clusters contain thousands and even tens of thousand member galaxies. Examples of rich regular clusters are the Coma cluster and the Perseus cluster. No regular cluster is found reasonably close to our Galaxy than the Coma cluster which is at a distance of approximately 100 Mpc (Kent and Gunn, 1982). It is the a very rich cluster containing 10,000 galaxies or more, and owing to its nearness it has become the best observed one among the regular clusters.

1.4.2 Historical observation of dark matter

In 1932, Jan Oort make a study on the motion of neighbouring stars where the gravitaional effect recieved from the stars within the galaxy's disk allowed him to provide a measure of the disk's mass (Oort, 1932). The mass of the disk he obtained was twice the mass in stars and nebulae which led him to conclude that there has to be more mass than is seen as bright stars. He concluded that this mass belongs to the stars that are to dim to be seen.

Extragalactic DM was discovered by Zwicky (1933) only a year after Oort's original study of the DM near the Sun (Sciama, 1993). Zwicky observed the coma cluster and eximined its dynamics by assuming that galaxies are virialized. His observation gave evidence for the total mass required to keep the galaxy cluster gravitationally bound to be more that 100 times that of the stars in all its galaxies.

There are a number of evidences for the existance of DM in galaxies and galaxy clusters. Mass determinations are very important as they measure the amount and distribution of DM in clusters indirectly. The existance of DM is obtained only indirectly from its gravitational effect on the visible matter, radiation and large

scale structure of the Universe. On small (microscopic) scales DM is believed to show weak interactions and this gives hope that it may be detected in low energy particle physics experiments.

In the following two subsections we shall discuss the existance of DM through the rotational curve of a galaxy and gravitational lensing effect of a galaxy cluster.

1.4.3 Rotation curve of a galaxy

The most convincing and direct evidence for DM on galactic scales comes from the observations of the rotation curves of galaxies, namely the graph of circular velocities of stars and gas as a function of their distance from the galactic center (Bertone et al.). In 1970's Vera Rubin measure the rotation curve of stars and gas in several galaxy clusters. Observed rotation curves usually exhibit a characteristic flat behavior at large distances, i.e, out towards, and even far beyond, the edge of the visible disk see Fig. 1.3.

In Newtonian dynamics the circular velocity is expected to be

$$v(r) = \sqrt{\frac{GM(r)}{r}}, \tag{1.9}$$

where, as usual, M(r) = $4\pi \int \rho(r) r^2$ dr, and ρ(r) is the mass density profile, and should be falling $\propto 1/\sqrt{r}$ beyond the optical disc. The fact that v(r) is approximately constant implies the existence of a halo with M(r) $\propto$ r and $\rho \propto \frac{1}{r^2}$ (Bertone et al.).

If the rotation curve of the spiral galaxy is flat, v_{rot} = constant, M($\leq$ r) $\propto$ r and so the mass within radius r increases linearly with distance from the centre. This contrasts dramatically with the distribution of light in the discs, bulges and halos of spiral galaxies which decrease exponentially with increasing distance from the centre. Consequently, the local mass-to-luminosity ratio must increase in the outer regions of spiral galaxies.

It is most convenient to quote the results in terms of mass-to-luminosity ratios relative to that of the Sun. For the visible parts of spiral galaxies, for which the rotation curves are well determined, mean mass-to-light ratios in the B waveband are in the range 1-10. This is similar to the value found in the solar neighbourhood; averaging over the masses and luminosities of the local stellar populations, a value

of M/L $\approx$ 3 is found. The M/L ratio must however increase to much larger values at large values of r. Values of M/L $\approx$ 10-20 $M_{\odot}/L_{\odot}$ are found in the outer regions of spiral galaxies, similar to the values found for elliptical galaxies. These data provide crucial evidence for the presence of DM in galaxies. (Longair, 2011).

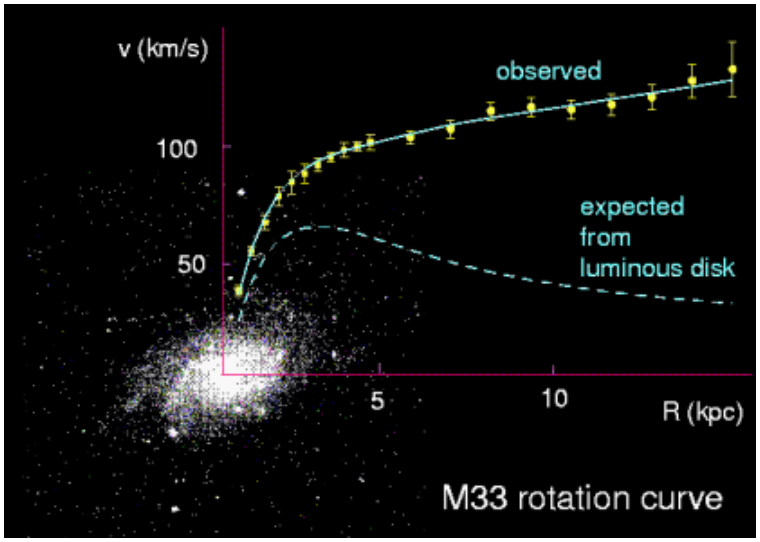

Figure 1.3: The observed rotational speed of a galaxy in comparison with what is expected from its luminous disk (Hernandez et al., 2015)

1.4.4 Gravitational lensing by galaxy clusters

Gravitational lensing is the gravitational bending of light emitted by a background source by an object, i.e, a galaxy or galaxy cluster which acts like a lens between the observer and the source. Measurement of matter distributions in galaxies and galaxy clusters obtained using strong gravitational lensing effect has provided strong evidence for the existence of DM within the Universe. The cores of galaxy clusters are dense enough to produce strong gravitational lensing, giving rise to strongly distorted images of background galaxies (Kaiser and Squires, 1993). If the source, lensing object and observer are aligned, then the observer will see the light from the source smeared in a circle with the lens in its centre which is known us "Einstein ring". From measurement of position and strength of the lensing object one can determine the angular radius of the "Einstein ring" θ_E using the relation:

$$\theta_E = \sqrt{\frac{4GM}{c^2}\frac{D_{LS}}{D_L D_S}} \tag{1.10}$$

where D_L, D_S and D_{LS} are the angular diameter distance to the lensing object or deflector, background source, and between them, respectively as shown in the Fig. 1.4. Thus the measurement of the distance to the lensed object and the source will allow an estimate for the total mass, M, of the lensing object (Metcalf and Madau, 2001). Once the total mass of the lensing object is determined, it can be used directly to obtain an estimate for the amount of DM within galaxy and galaxy clusters.

From observations it is seen that gravitational lensing obtained from a galaxy

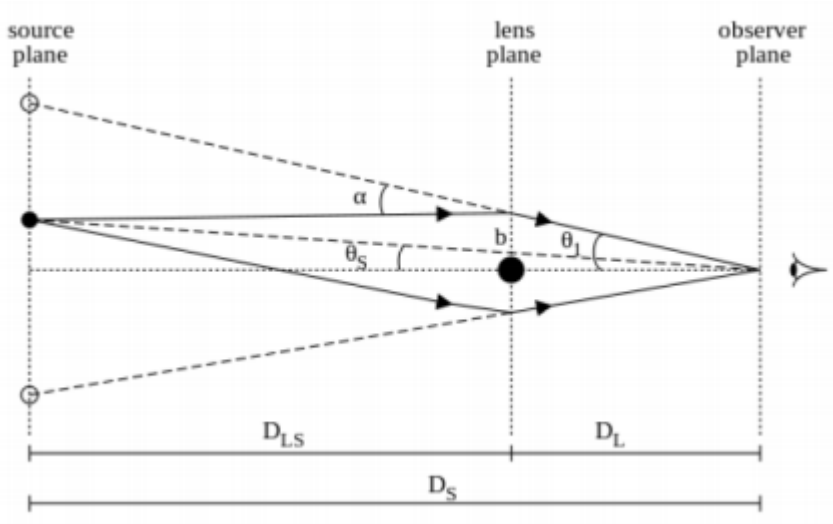

Figure 1.4: Graphical representation of gravitational lensing process. Image adapted from (Luković et al., 2014)

.

cluster implied the existance of extra matter than the visible one because the visible matter by itself cannot cause this much amount of bending. This extra matter is named DM because of its non-luminuos nature.

1.5 Composition of dark matter

As measurements by Planck reveal only about 4.9% of our Universe is visible (luminous) while 26.8% of it is DM and the rest which is about 68.3% is dark energy (see Fig. 1.2). The invisiblity of the DM is attributed to the fact that either it is emitting little radiation or it has no radiation at all. According to this fact the DM could merely be ordinary material, such as ultrafaint stars, large or small black holes, cold gas, or dust scattered around the universe - all of which emit or reflect

too little radiation for our instruments to detect. It could even be a category of dark objects known as MACHOs (MAssive Compact Halo Objects) that lurk invisibly in the halos surrounding galaxies and galactic clusters. On the other hand, DM could consist of exotic (unfamiliar) particles that we have not figured out how to observe. Physicists theorize about the existence of these particles, although experiments have not yet confirmed their presence (Rubin, 1998). It is convenient to consider separately the possibilities that the DM is baryonic or non-baryonic.

1.5.1 Baryonic dark matter

By baryonic matter, we mean ordinary matter composed of protons, neutrons and electrons. Certain forms of baryonic matter are very difficult to detect because they are very weak emitters of electromagnetic radiation. Examples of such weak emitters are brown dwarf stars with masses $M \leq 0.08\ M_{\odot}$, in which the central temperatures are not hot enough to burn hydrogen into helium. Although brown dwarfs are estimated to be about twice as common as stars with masses $M \geq 0.08\ M_{\odot}$, they contribute very little to the mass density in baryonic matter as compared with normal stars because of their low masses. The consensus of opinion is that brown dwarfs could only make a very small contribution to the DM.

Black holes are another possibility for the DM. The supermassive black holes in the nuclei of galaxies have masses which are typically only about 0.1% of the mass of the bulges of their host galaxies and so they contribute negligibly to the mass density of the Universe. There might, however, be an invisible intergalactic population of massive black holes. Limits to the number density of such black holes can be set in certain mass ranges from studies of the numbers of gravitationally lensed images observed in large samples of extragalactic radio sources. The upper limit to the cosmological mass density of these black holes corresponded to less than 1% of the critical cosmological density (Wilkinson et al., 2001).

An impressive approach to setting limits to the contribution which discrete low mass objects, known as MAssive Compact Halo Objects, or MACHOs, could make to the DM in the halo of our own Galaxy, has been the search for gravitational microlensing signatures of such objects as they pass in front of background stars. The MACHOs include low mass stars, white dwarfs, brown dwarfs, planets and black holes. These lensing events are very rare and so very large numbers of background stars have to be monitored. This technique is sensitive to MACHOs

with a very wide range of masses, from 10^{-7} to 100 $M_{\odot}$. In addition, the expected light curve of such gravitational lensing events has a characteristic light curve which is independent of wavelength. The time-scale of the brightening is roughly the time it takes the MACHO to cross the Einstein radius of the dark deflector. The first example of such a microlensing event was discovered in October 1993, the mass of the invisible lensing object being estimated to lie in the range $0.03 < M < 0.5\ M_{\odot}$ (Alcock et al., 1993).

By the end of the MACHO project, 13 definite and four possible events were observed in the direction of the Large Magellanic Cloud, significantly greater than the 2 - 4 detections expected from known types of star. The best statistical estimates suggest that the mean mass of these MACHOs is between 0.15 and 0.9 $M_{\odot}$. The statistics are consistent with MACHOs making up about 20% of the necessary halo mass. Somewhat fewer microlensing events were detected in the EROS project which found that less than 25% of the mass of the standard DM halo could consist of dark objects with masses in the range 2×10^{-7} to 1 $M_{\odot}$ at the 95% confidence level. The consensus view is that MACHOs alone cannot account for all the DM in the halo of our Galaxy and so some form of non-baryonic matter must make up the difference (Longair, 1994).

1.5.2 Non-baryonic dark matter

Most of the DM is probably extraordinary matter, which is of non-baryonic form, consisting of undiscovered particles. Three of the most popular candidates are axions, neutrinos with finite rest mass and Weakly Interacting Massive Particles, or WIMPs.

i. Axions

The smallest mass candidates are the axions which were invented by particle theorists in order to "save quantum chromodynamics from strong CP violation". If they exist, they must have been created when the thermal temperature of the Universe was about 10^{12} K but they were out of equilibrium and never acquired thermal velocities - they remained "cold". Their rest mass energies are expected to lie in the range 10^{-2} - 10^{-5} eV. The role of such particles in cosmology and galaxy formation is discussed in Kolb and Turner (1990).

ii. Neutrinos with finite rest mass

A second possibility is that the three known types of neutrino have finite rest masses. Laboratory tritium β - decay experiments have provided an upper limit to the rest mass of the electron antineutrino of $m_\nu \leq 2$ eV (Weinheimer, 2003), although the particle data book suggests a conservative upper limit of 3 eV. The discovery of neutrino oscillations has provided a measurement of the mass difference between the μ and τ neutrinos of $\Delta\, m_\nu^2 \sim 3 \times 10^{-3}$ (Eguchi et al.), (Aliu et al., 2005). These two results are then combined to provide the following upper limit for their relic density:

$$\Omega_\nu h^2 = 0.07, \tag{1.11}$$

this value thus clearly shows that neutrinos cannot be a dominant component of DM. Their mass limit also implies they are relativistic collisionless particles that they would freely stream on scale of about 40 Mpc, as a result of which they would erase the observed density fluctuations on such scale. Moreover simulation results have also shown that the clustering we see today in the Universe cannot fit this picture.

iii. WIMPs

A third possibility is that the DM is in some form of Weakly Interacting Massive Particle, or WIMP. WIMPs are believed to exist in thermal equilibrium in abundance in the early Universe when

$$K_B T = m_\chi c^2 \tag{1.12}$$

where T and m_χ are the temperature of the Universe and WIMP mass, respectively and K_B is the boltzmann constant. The abundance of WIMPs is preserved as the number of forward process is equal to the backward process:

$$\chi\overline{\chi} \leftrightarrows l\bar{l} \tag{1.13}$$

However, as the temperature falls (i.e, $T < m_\chi$) the equilibrium abundance also falls exponentially until the rate of forward process falls below the Hubble expansion rate, $H = \frac{\dot{R}}{R}$. At this point, the WIMP cease to annihilate, they fall out of equilibrium,

and a relic cosmological abundance remains.

The time evolution of the number density $n_\chi(t)$ of WIMPs is given by the Boltzmann equation (Lisanti, 2017).

$$\frac{dn_\chi}{dt} + 3Hn_\chi = - < \sigma_A v > [(n_\chi)^2 - (n_\chi^{eq})^2], \tag{1.14}$$

where the first term in brackets on the right-hand side of Eqn. 1.14 accounts for depletion of WIMPs due to annihilation, and the second term arises from creation of WIMPs from the inverse reaction. The equilibrium abundance is obtained when the rate for depletion is equal to creation of particles. The flux of the DM particles per unit time from a unit volume V containing them is given by

$$\Gamma_{ann} = \left(\int \frac{\rho_{DM}^2}{m_\chi^2} dV \right) \times (\sigma_A v) \times N_{SM} \tag{1.15}$$

which is a product of three terms, the number of DM particle pairs in the volume V, the DM pair annihilation rate, and the flux of SM particles per annihilation event respectively. In equilibrium the DM annihilation rate can be understood to be Γ_{ann} = n_χ^{eq} < σ_A v >, where n_χ is the equilibrium WIMP number density and <σ_Av> is the DM pair annihilation rate.

For typical values of temperature, T $\sim \frac{m_\chi}{20}$ and <σ_Av> $\sim \frac{\alpha^2}{m^2}$, we obtain the present day mass density in units of the critical density, ρ_c, contributed by the DM to be

$$\Omega_\chi h^2 = \frac{n_\chi m_\chi}{\rho_c} \simeq \frac{3 \times 10^{-27} cm^3 s^{-1}}{< \sigma_A v >} \simeq 0.1 (\frac{0.01}{\alpha})^2 (\frac{m_\chi}{100 GeV})^2. \tag{1.16}$$

Eqn. 1.16 shows that a weakly interacting DM particle (i.e., $\alpha \sim 0.01$ and mass m_χ $\sim$ 100 GeV) gives the correct abundance today as measured for example by Planck (Ade et al., 2016). This match which is known as the "WIMP miracle" will thus give a possibility to set limit on the annihilation cross-section or lifetime of the WIMP.

1.6 Detection mechanisms

1.6.1 Direct detection of dark matter

Direct detection experiments appear today as one of the most promising techniques to detect particle DM. The idea is very simple: if the galaxy is filled with WIMPs,

then many of them should pass through the Earth, making it possible to look for the interaction of such particles with matter, e.g. by recording the recoil energy of nuclei, as WIMPs scatter off them (Lisanti, 2017).

The key ingredients for the calculation of the signal in direct detection experiments are the density and the velocity distribution of WIMPs in the solar neighborhood and the WIMP-nucleon scattering cross section. With this information, it is then possible to evaluate the rate of events expected in an experiment (i.e, WIMP-nucleon scattering events) per unit time, per unit detector material mass.

The rate is approximately given by

$$R \approx \sum_i N_i n_\chi < \sigma_{i\chi} > \tag{1.17}$$

where the index, i, runs over nuclei species present in the detector

$$N_i = \frac{Detector\ mass}{Atomic\ mass\ of\ species\ i}$$

is the number of target nuclei in the detector,

$$n_\chi = \frac{WIMP\ energy\ density}{WIMP\ mass}$$

is the local WIMP density and <$\sigma_{i\chi}$> is the cross section for the scattering of WIMPs off nuclei of species i, averaged over the relative WIMP velocity with respect to the detector (Lisanti, 2017).

The type of scattering process can be elastic or inelastic scattering. The elastic scattering of a WIMP off of a nucleus in a detector is simply the interaction of the WIMP with a nucleus as a whole, causing it to recoil, ideally often enough to measure the recoil energy spectrum in the target. With a Boltzman velocity distribution of WIMPs, centered at 270 km/s, the spectrum of recoils is exponential with typical energies of <E> $\sim$ 50 keV. Current experiments can detect recoils of considerably lower energy, as low as 1 - 10 keV. Inelastic scattering, on the other hand, is not observed by the recoil of a target nuclei. Instead, the WIMP interacts with orbital electrons in the target either exciting them, or ionizing the target. Alternatively, the WIMP could interact with the target nuclei leaving it in an excited nuclear state. This process leaves the signature of a recoil followed by the emission of a photon a nanosecond, or so, later (Bertone et al.).

1.6.2 Indirect detection of dark matter

Indirect detection of DM is the technique of observing the radiation produced in DM annihilations. The flux of such radiation is proportional to the annihilation rate, which in turn depends on the square of the DM density, $\Gamma_A \propto \rho^2_{DM}$. Therefore, the "natural" places to look at, when searching for significant fluxes, are the regions where large DM densities accumulate. This regions are referred as amplifiers. Dense regions of the galactic halo, such as the galactic center, may be excellent amplifiers for the purposes of detecting gamma rays or neutrinos. Annihilation products which are charged move under the influence of magnetic fields making it impossible to consider point sources of such radiation. Despite this, observations of cosmic positrons and anti-protons can be valuable tools in searching for particle DM (Bertone et al.).

1.6.3 Detection from particle colliders

Due to their lack of electromagnetic interactions, non-baryonic nature and therefore weak Standard-Model interactions, DM particles escape detection at colliders in a similar way as neutrinos. As a consequence, they produce a characteristic signal of missing energy. At hadron colliders such as the Large Hadron Collider (LHC), only the missing transverse energy, E_T, can be observed, since the longitudinal momentum fractions of the incoming partons in the colliding hadrons are unknown. The missing E_T is then determined from the recoiling observed objects such as jets, heavy quarks, photons and leptons (Klasen et al., 2015).

1.7 Summary

In this chapter we paved a way to our very topic which is dark matter (DM). We start by setting two fundamental principles of cosmology, i.e. the homogenity and isotropy of our Universe. This principles make it easy to come up with different models of the Universe among which the Hot Big Bang model is the most accepted one. The matter energy budget of the Universe tell us that about 95% of the Universe is invisible of which DM takes 26%. Astronomic observations make us certain about the exitances of this DM whose influence is seen on the visible matter. And finally, we have introduced the possible DM candidates and indicated the three detection mechanisms.

CHAPTER 2

Diffused radio emissions from galaxy clusters

2.1 Introduction

Clusters of galaxies are the largest gravitationally bound systems in the Universe, with typical masses of about 10^{15} $M_{\odot}$, and volumes of about 100 Mpc^3. Most of the gravitating matter in any cluster is in the form of DM ($\sim 80\%$). Some of the luminous matter is in galaxies ($\sim 3\%$ - 5%), the rest is in diffuse hot gas ($\sim 15\%$ - 17%). This thermal plasma, consisting of particles of energies of several keV, is commonly referred to as Intracluster Medium (ICM). Clusters are formed by hierarchical structure formation processes. In this scenario, smaller units (galaxies, groups and small clusters) formed first and merged under gravitational pull to larger and larger units in the course of time. Cluster mergers are the mechanism by which clusters are assembled. Denser regions form a filamentary structure in the Universe, and clusters are formed within filaments, often at their intersection, by a combination of large and small mergers. Major cluster mergers are among the most energetic events in the Universe since the Big Bang . During mergers, shocks are driven into the ICM, with the subsequent injection of turbulence. The merger activity, which has characterized much of the history of the Universe, appears to be continuing at the present time and explains the relative abundance of substructure and temperature gradients detected in clusters of galaxies by optical and X-ray observations (Feretti et al., 2012).

There are a number of observational results obtained recently related to the diffuse radio sources from galaxy clusters. In this chapter we will discuss about this diffuse and extended radio emission from galaxy clusters and we present the approach used by three models to explain the possible sources for the relativistic electrons which are responsible for this extended emission.

2.2 Diffused radio emissions in galaxy clusters

Galaxy clusters are characterized by emission in the radio band among others. Obvious radio sources are the individual galaxies, whose emission has been observed in recent decades with sensitive radio telescopes. It often extends well beyond the galaxy optical boundaries, out to hundreds of kpc, and hence it is expected that the radio emitting regions interact with the ICM. This interaction is indeed observed in tailed radio galaxies, and radio sources filling X-ray cavities at the centre of cool core clusters (Feretti and Giovannini, 2008). More puzzling are diffuse extended radio sources, which cannot be obviously ascribed to individual galaxies, but are instead associated with the ICM. This radio emission represents a striking feature of clusters, since it demonstrates that the thermal ICM plasma is mixed with non-thermal components. Such components are large scale magnetic fields with a population of relativistic electrons in the cluster volume.

In recent years, there has been growing evidence for the existence of cluster large scale diffuse radio sources, of synchrotron origin, which have no optical counterpart and no obvious connection to the cluster galaxies, and are therefore associated with the ICM Ferrari et al. (2008). The first diffuse radio source detected in a cluster of galaxies is the giant radio halo at the center of the Coma cluster (Large et al., 1959). Several years later, extended diffuse emission was also detected at the periphery of the Coma cluster and at the center of the Perseus cluster. Nowadays, diffuse radio emission with surface brightness down to 0.1 μ Jy arcsec^{-2} at 1.4 GHz is known in about 80 clusters, under several cluster evolutionary conditions (merging and relaxed clusters), at different cluster locations (center, periphery, intermediate distance), and on very different size scales from 100 kpc to > Mpc (Feretti et al., 2012). Galaxy cluster regions which show diffuse synchrotron emission are in general divided into radio halos and radio relics see Fig. 2.1. Radio halos and relics are faint (μ Jy/arcsec^2 at 1.4 GHz) sources extended on Mpc scales, located at the center and in the outskirts of about 100 merging galaxy clusters, respectively. The study of radio halos and relics is of paramount importance to shed light on the history and physical properties of galaxy clusters, and to clarify the role of non-thermal components associated to the ICM. Their nature reveals very weak large-scale magnetic fields, with central strengths $\sim \mu$G, fluctuation scales of up to several hundreds of kpc, and rarefied, very energetic populations of relativistic electrons spread across the cluster volume (Feretti et al., 2012).

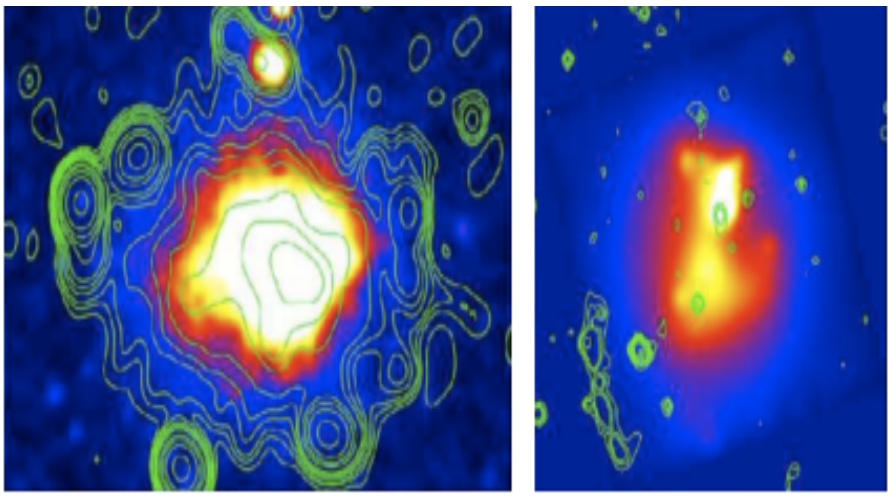

Figure 2.1: Image of radio halos (left) and radio relics (right) showing the extended diffuse radio emission at the cluster center and periphery, respectively. Image adapted from (Perez-Torres et al., 2009)

There are two observables about the diffused radio spectrum i.e, the integrated radio spectra and the spatial variation of the spectral index. The integrated radio spectra of halo sources are still poorly known. The difficulty of spectral studies are that i) only in a few cases the spectrum is obtained with more than three flux density measurements at different frequencies, ii) for most sources the highest available frequency is 1.4 GHz, therefore it is difficult to determine the presence of a spectral steepening, crucial to discriminate between different reacceleration models. The best studied integrated radio spectrum is that of the Coma cluster where clear evidence of a high frequency steepening is present (see Fig. 2.2 and (Thierbach et al., 2003) for a detailed discussion).

A powerful tool to understand the physical properties of radio halos is the spectral index map. It reflects the variation of the shape of the electron energy distribution (see Eq. 2.2) and of the magnetic field in which they emit. Measurment of the spatial distribution of spectral index of the radio emission from the DM annihilation within the galaxy cluster provides a valuable physical information for understanding the structure of the DM in the cluster. Mapping the spatial distribution of spectral index represents a powerfull tool to study the properies of the relativistic electrons and the magnetic field in which they emit and investigate the connection between the electron energy distribution and the ICM (Vacca et al., 2014). The first spectral

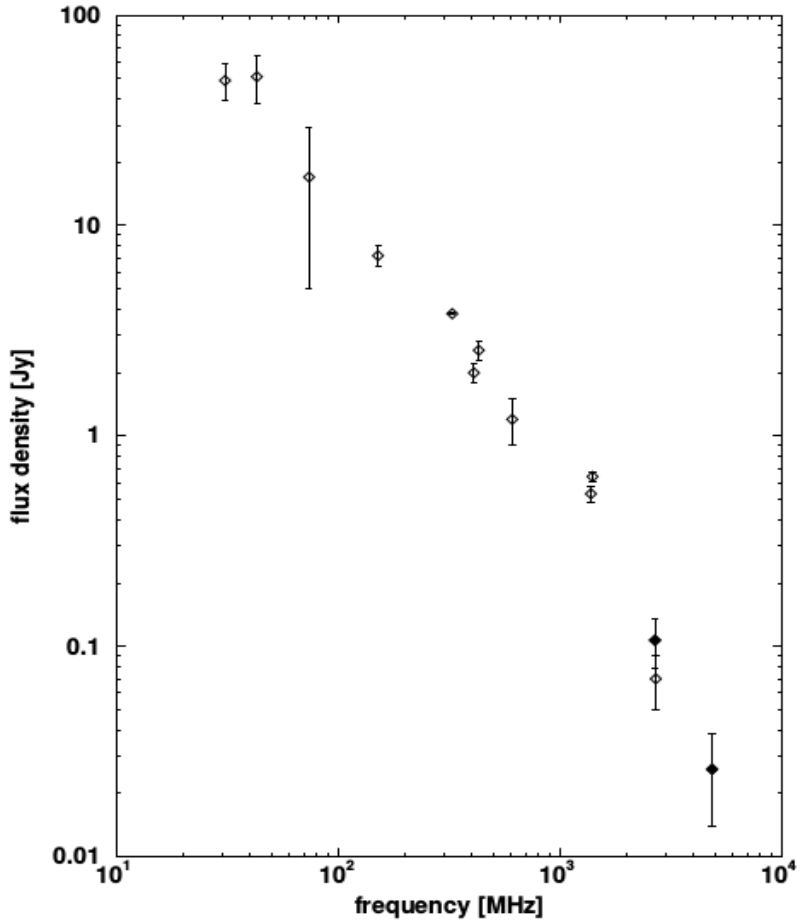

Figure 2.2: Integrated radio continuum spectrum of the diffuse radio halo source Coma C. The filled dots represent new observations made by (Thierbach et al., 2003).

index map of a radio halo was obtained for the Coma cluster (Giovannini et al., 1993). The spectral distribution is smooth with a steepening from the center to the peripheral regions, where the spectral index is $\alpha \sim 2$. The spectral index images of giant radio halos in A665 and A2163, with an angular resolution $\sim 1'$, show flattening and patches, and radial steepening in the undisturbed cluster regions (Feretti et al., 2004). Spectral variations are likely to reflect the energy losses/gains of the radiating electrons. The spectral index is given by the formula:

$$\alpha = \frac{ln(F_1/F_2)}{ln(\nu_1/\nu_2)}, \tag{2.1}$$

Where F_1 and F_2 are flux values at frequencies ν_1 and ν_2 respectively.

The spectral index can be used to determine the electron energy distribution given

by:

$$N(E)dE = N_0 E^{-\delta}, \tag{2.2}$$

where the injection spectral index, δ of the electron energy distribution is related to the spectral index through δ = 2α + 1.

2.3 Models for the origin and evolution of particles giving rise to diffuse sources

Since magnetic fields are found to be ubiquitous in galaxy clusters a very crucial ingredient for the existence of diffuse synchrotron radio sources is the presence of relativistic particles. Radio halos are most difficult to explain, because of their very large size. Radiating electrons cannot travel such large distances within their lifetime, because of strong radiative losses by synchrotron and inverse Compton emission. Three main classes of models have been suggested for the origin of relativistic electrons present in the cluster volume and responsible for the diffuse radio emission: the primary electron model which predict that relativistic particles are continuously accelerated in the cluster volume, the secondary electrons model in which relativistic electrons are produced throughout the cluster by pp collisions and a model that suggests DM annihilation processes as a source of relativistic electrons.

2.3.1 The primary electron model

Primary relativistic electrons are present in the cluster volume, because they were injected by AGN activity and radio galaxy during the cluster dynamical history. This population of electrons suffer strong radiation loss mainly due to synchrotron and inverse Compton emission, thus reacceleration is needed to maintain their energy to the level necessary to produce the observed synchrotron radio emission in relatively weak magnetic fields(Markevitch et al., 2005). Some of the shortcomings of the primary electrons model are the electrons have short life-time as compared to the age of the cluster and, as a result of the energy losses, they travel short distance as compared to the size of a radio halo (Roettiger et al., 1999). Primary electron models can also be referred to as reacceleration models. There are two main ways that entail the transfer of energy from the cluster ICM to the radiating particles: these are cluster turbulence and cluster shocks.

i. Reacceleration by turbulence:

Simulations show that during cluster mergers, turbulence is generated throughout the cluster over $\sim$ Mpc scales. Energy can thus be transferred from the ICM into the non-thermal component through the interaction of electrons with MHD turbulence. The emerging scenario is that turbulence reacceleration is likely the major mechanism responsible for the supply of energy to the electrons radiating in radio halos. The time during which the process is effective is relatively short (a few 10^8 years), so that the radio emission is expected to correlate with ongoing or most recent merger event (Feretti et al., 2004). The evidence of the presence of faint diffuse magnetic fields in all galaxy clusters, the behaviour of radio spectra, the existence of ultra-steep radio halos, the correlation between radio spectra and temperature, the association between radio halos and cluster mergers, and the fact that halos are not common in galaxy clusters, are supportive of primary electron models for radio halos (Feretti et al., 2012).

ii. Reacceleration by shocks:

The acceleration occurs diffusively, in that particles scatter back and forth across the shock, gaining at each crossing and recrossing an amount of energy proportional to the energy itself. The acceleration efficiency is mostly determined by the shock Mach number. Current observations globally favour the scenario that cluster shocks are strictly linked to relics. Accelerated electrons have been suggested either to be thermal ICM electrons, or relativistic electrons released by a former active radio galaxy. Because of the short electron radiative lifetimes, radio emission is produced close to the location of the shock waves. These models also predict that the magnetic field within the relic is aligned with the shock front, and that the radio spectrum is flatter at the shock edge, where the radio brightness is expected to decline sharply. These expectations are consistent with the classic elongated structure of relics, almost perpendicular to the merger axis, and their polarization properties (Vazza et al., 2012) show that the detection frequency of radio relics and the fact that they are also detected in cluster peripheries is consistent with their link to shocks.

2.3.2 The secondary electron model

In the hadronic model, secondary electrons are injected as secondary particles by inelastic nuclear collisions between the relativistic protons and the nuclei of the thermal ambient intracluster medium. The protons diffuse on large scale because their energy losses are negligible. They can continuously produce in situ electrons, distributed through the cluster volume. The reactions that lead to the production of secondary electrons are described by the secondary electron model:

$$p + p \longrightarrow \pi^{\pm} + X$$

where X represents any reachable final state from the initial state. The charged pions ($\pi^{\pm}$) will decay into electrons, positrons and neutrinos via muons;

$$\pi^{+} \longrightarrow \mu^{+} + \nu_{\mu}$$

$$\pi^{-} \longrightarrow \mu^{-} + \overline{\nu}_{\mu}$$

and

$$\begin{aligned} \mu^{+} &\longrightarrow e^{+} + \nu_{e} + \overline{\nu}_{\mu} \\ \mu^{-} &\longrightarrow e^{-} + \overline{\nu}_{e} + \mu \end{aligned} \tag{2.3}$$

Similarly, the neutral pions (π^{0}) will decay predominantly into γ-rays:

$$\begin{aligned} p + p &\longrightarrow \pi^{0} + X \\ \pi^{0} &\longrightarrow \gamma + \gamma \end{aligned} \tag{2.4}$$

Secondary electron models can reproduce the basic properties of the radio halos provided that the strength of the magnetic field averaged over the emitting volume is larger than a few μG (Brunetti et al., 2001). In this case, they predict synchrotron power-law spectra, which are independent of cluster location, i.e. do not show any features and/or radial steepening, and the spectral index values are flatter than $\alpha \sim 1.5$. Some of the problems of the secondary model include, the steepening at high frequencies of the Coma radio halo spectrum, the change of the spectral index along the cluster, and the worst problem being the lack of gamma ray detection.

2.3.3 Dark matter annihilation/decay processes

The third model suggested as a possible source of relativistic secondary electrons and positrons is from DM annihilation/decay processes in the galaxy clusters. In

this model DM annihilation/decay processes are believed to produce a wide range of SM particles and radiations such as electrons, positrons and gamma-ray radiations. Electrons and positrons will undergo energy losses while interacting with particles in ICM and will emit in a multiwavelength spectrum after reaching equilibrium states through various emission mechanisms (see section 3.3). A number of DM particle candidates have been proposed in the light of particle physics models, which are expected to produce indirect signals through annihilation/decay processes. WIMPs are the largest class of cold DM candidates among which neutralinos are the most stable particles that arise in extensions of the SM particle physics, see (Jungman et al., 1996) for more. Neutralinos are called Majorana type of particles, thus they are their own anti-particles. Through their self-annihilation they produce unstable SM particles such as neutral and charged pions (Colafrancesco et al., 2006). This neutral and charged pions will then decay into radiation (gamma rays) and particles (relativistic $e^{\pm}$), respectively. When these secondary $e^{\pm}$ interact with the magnetic field and charged particles in the intra-cluster medium (ICM) they produce radio signals through synchrotron emission processes, and gamma rays from bremsstrahlung and Inverse Compton Scattering (ICS) processes (see Fig. 2.3 below).

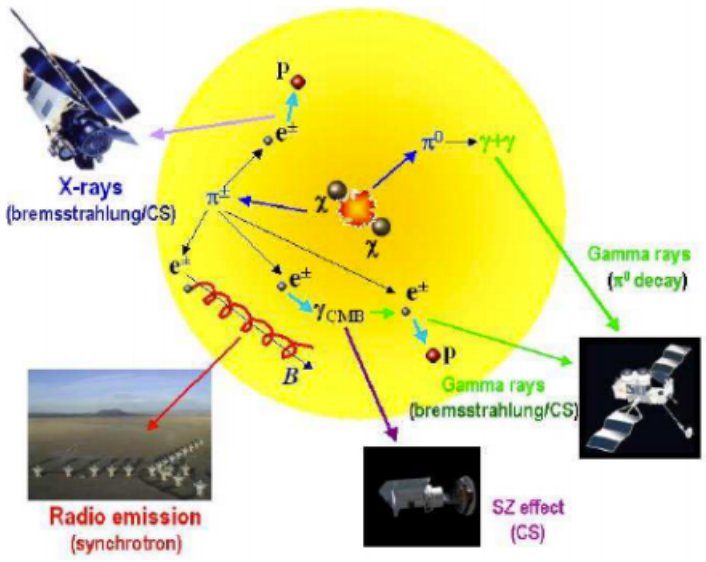

Figure 2.3: Graphical representation of multi-wavelength emission from neutralino annihilation process (Image adapted from (Colafrancesco et al., 2006))

.

Several authors have studied the astrophysical results of these assumptions laid on secondary electrons from DM annihilation/decay processes such as (Colafrancesco and Melé, 2001); and many more. One common strength of these previous studies lies in their ability to reproduce the observed steepening in the flux spectrum, the spectral energy distribution, at higher radio frequencies of the Coma cluster. This can be understood to be due to the fact that the spectrum of secondary electrons steepens when the energy of the electrons is comparable to the mass of neutralinos (Perez-Torres et al., 2009).

2.4 Summary

The main concern of this chapter has been the observed radio emission from clusters which is not related to the individual galaxies of the clusters. However, at present the origins of these diffuse extended non-thermal emission in galaxy clusters is not well understood. The source of this relativistic electrons which are responsible for the radio emission were suggested by different models. According to the primary model the transfer of energy from the cluster ICM to the radiating particles is due to the cluster turbulence and cluster shocks. In the hadronic model the secondary electrons are injected as secondary particles by inelastic nuclear collisions between the relativistic protons and the nuclei of the thermal ambient intracluster medium. According to the third model, which is the interest of this work, the source of the relativistic electrons is the DM annihilation processes in the galaxy clusters.

CHAPTER 3
Data presentation and analysis

3.1 Introduction

In order to study the diffused radio emission from galaxy clusters we considered DM annihilation/decay processes as a source of relativistic electrons. We applied this model on a sample of simulated Coma like galaxy clusters obtained from cosmological simulations. Cosmological simulations are a powerful and important tool in order to understand the cosmos. A detailed simulation can provide a means for grasping processes which occur on such long time scales (millions or billions of years) that it is not possible to observe these events in the Universe. Cosmological simulations are used to study galaxy collisions and also the formation of large scale structure in the Universe (Ruphy, 2011). In the following paragraphs we have introduced three cosmological simulation datasets avialable from which we have selected one for the purpose of our work.

Among many cosmological simulations is the GADGET, which is a simulation code for galaxy collisions or for early structure formation in the Universe (for more visit:`Cosmologicalsimulations-Wikiversity.html`). The GADGET computes gravitational forces with a hierarchical tree algorithm (optionally in combination with a particle-mesh scheme for long-range gravitational forces) and represents fluids by means of smoothed particle hydrodynamics (SPH) (Springel, 2005). The code can be used for studies of isolated systems, or for simulations that include the cosmological expansion of space, both with or without periodic boundary conditions. (visit:`CosmologicalsimulationswithGADGET.html`).

The most accurate cosmological simulation to date of the evolution of the large-scale structure of the Universe is the Bolshoi simulation (Klypin et al., 2011). The principal purpose of the Bolshoi simulation is to compute and model the evolution of dark matter halos, thereby rendering the invisible visible for astronomers to

study, and to predict visible structure that astronomers seek to observe (Rodríguez-Puebla et al., 2016). Bolshoi has given cosmologists a fairly accurate picture of how the Universe actually evolved. It is currently being analyzed in preparation for publication and distribution of its results in 2014. For further information visit: `BolshoiCosmologicalSimulation-Wikipedia.html`.

MUltidark SImulation of galaxy Clusters (MUSIC)-dataset is a large subset of a mass limited sample of resimulated clusters selected from the MultiDark Simulation which is a DM only N-body simulation with 2048^3 particles in a 1 h^{-1} Gpc cubic box. This simulation run was done using the best-fit cosmological parameters to WMAP7 + BAO + SNI (Ω_M = 0.27, Ω_b = 0.0469, Ω_Λ = 0.73, σ_8 = 0.82, n = 0.95, h = 0.7) (Jarosik et al., 2011). The MUSIC clusters has a large numbers of samples (282 clusters and thousands of groups) and a high resolution (Sembolini et al., 2012).

3.2 Data presentation

For the purpose of our work (i.e, in order to determine the DM annihilation flux from neutralino χ in galaxy clusters) we have used the MUSIC-dataset as our first data source. The datas in the MUSIC simulation contain the particle mass and coordinates divided into different mesh or grids (i.e, 21, 101, 201, 401, or 801). From this large number of samples avialable on the MUSIC-dataset we have taken two simulated Coma like galaxy clusters namely, SGC280 and SGC282 where the sample selection was done to optimize the resolution and computation time. Therefore, our samples, SGC280 and SGC282 are both divided by 201 grids allowing us to obtain comparatively good resolution and low computation time.

The second data source that we have taken into account is the DarkSUSY package. The DarkSUSY package is a fortran package that calculate the yield of different particles per a neutralino annihilation. In this package the simulation is done for 8 "fundamental" annihilation channels $c\bar{c}$, $b\bar{b}$, $t\bar{t}$, $\tau^+\tau^-$, W^+W^-, Z^0Z^0, gg and $\mu^+\mu^-$ and different masses of neutralino (Gondolo et al., 2004). And for our specific case we have taken the production (initial) spectra (in other words, the yield of electrons per neutralino annihilation) for a neutralino mass of 35 GeV dominated by a $b\bar{b}$ species. For the latest version of DarkSUSY and for a more technical manual, visit the official DarkSUSY website, `http://www.physto.se/~edsjo/darksusy/`.

3.3 Modeling the radio emission

Since radio synchrotron emission is expected as a natural by-product of the self annihilation of super-symmetric DM particle, we have studied the synchrotron emission in galaxy clusters by considering the annihilation of neutralino which is mainly composed of $b\bar{b}$ species. We also have considered a neutralino mass of 35 GeV which has been tested in Mekuria et al. (2017) to be a viable model for the production of secondary electron responsible for the diffuse emission in galaxy clusters, with the annihilation rate of 1×10^{-26} cm^3 s^{-1} in two galaxy clusters located at a redshift of z = 0.028. For the annihilation channel we have considered a branching ratio of 1.

In the following subsections we present the necessary mathematical expressions that will help us to model the sychrotron emission from the annihilation process of WIMPs.

3.3.1 Dark matter distribution and magnetic field models

While discussing indirect detection mechanism of DM, it was stated that the DM particle annihilation rate is proportional to the square of DM density. Therefore, it is crucial to begin by specifing how we model the DM density taking the DM informations (masses of the DM particles and their positions) from the MUSIC-datasets. And then we used the smooth-particle-hydrodynamic (SPH) kernel to determine the DM densities on a grid (see section 3.4). In Fig. 3.1 we have shown the square of DM density maps for SGC280 and SGC282, which are produced for our galaxy clusters according to the dataset avialable on the MUSIC database. The brightest colors in the map clearly show enhanced DM density structures which are required to correctly determine emissions from DM annihilation processes in the cluster.

In order to determine the DM annihilation signals from the synchrotron emission we also need to model the magnetic field. In Mekuria et al. (2017) two magnetic field Models were used for this purpose, these are magnetic field Model A and Model B presented below:
(i) Model A is a model that evaluate the magnetic field strength from the gas distribution. The magnetic field profile in this case is given by

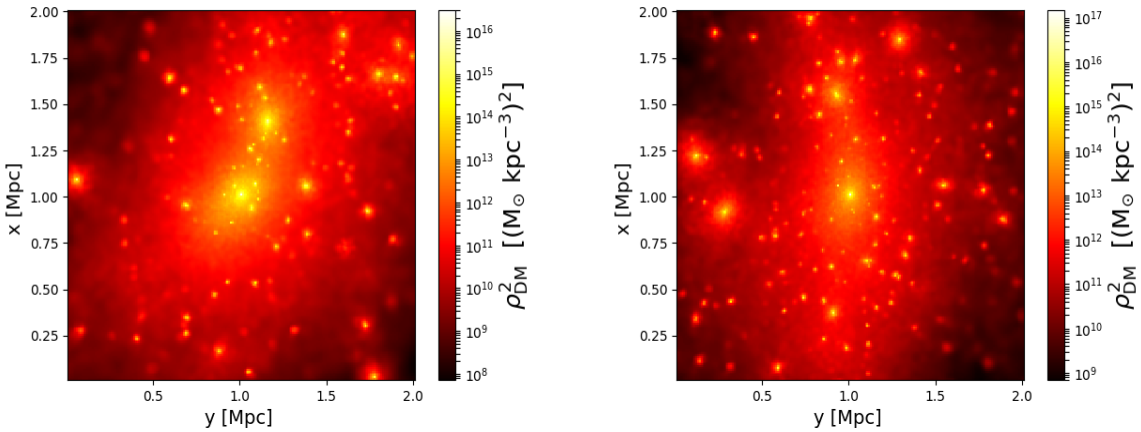

Figure 3.1: The DM density square map of the SGC280 (left) and SGC282 (right) according to the dataset avialable on the MUSIC database.

$$B(r) = B_0(1 + (r/r_s)^2)^{-q_b} \tag{3.1}$$

where B_0 is the central magnetic field strength of the Coma cluster, r is the radial distance from the cluster center, r_s is the scale radius of the DM density profile and q_b is scaling exponent choosen to be 0.5 (Colafrancesco et al., 2015).

(ii) Model B is a magnetic field model which uses the best observational value for a central magnetic field in the Coma Cluster equal to 4.7 μG (at electron number density of 3.44 $\times$ 10^{-3} cm^{-3}) from Bonafede et al. (2010). The magnetic field B of the galaxy cluster is related to the electron number density n_e by

$$B = 4.7\ \mu G(n_e/3.44 \times 10^{-3}\ cm^{-3})^{0.5} \tag{3.2}$$

The electron number density n_e in cm^{-3} is evaluated as in Sembolini et al. (2012),

$$n_e = N_e\rho_{gas}(1 - Z - Y_{He})/m_p, \tag{3.3}$$

where N_e, ρ_{gas}, Z, Y_{He} = 0.25 and m_p are the number of ionized electrons per hydrogen atoms, gas density, metallicity, helium concentration and proton mass, respectively.

We have considered magnetic field Model A following the conclusion from Mekuria et al. (2017) and determined the magnetic field strength in each cube of size 10 kpc.

The magnetic field profiles for these two magnetic field models discussed above are shown in Figure. 3.2.

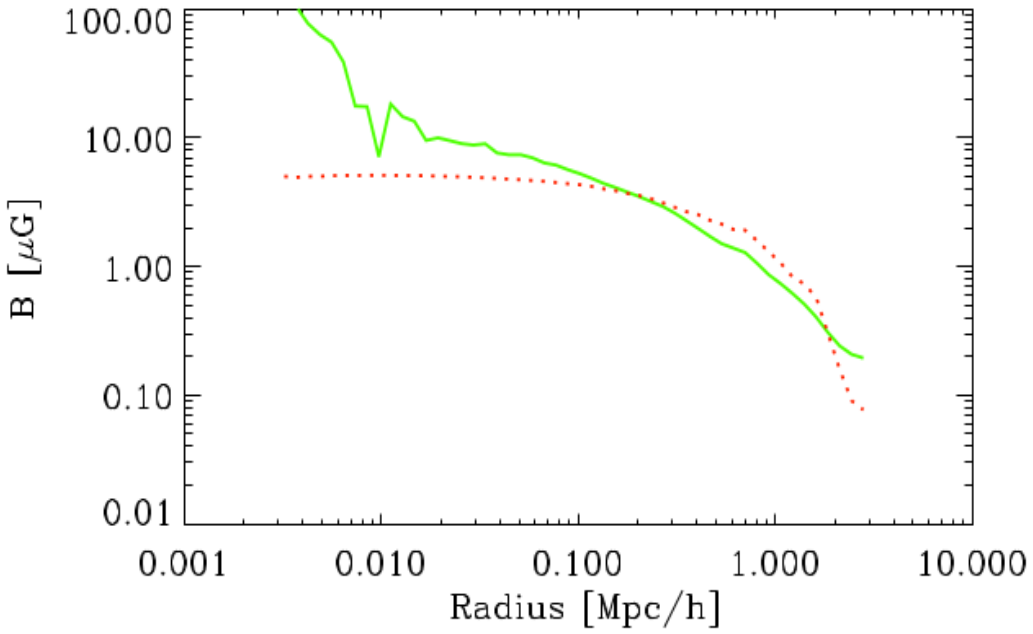

Figure 3.2: Magnetic field profiles of the two magnetic field models: Model A and Model B are shown in red dotted line and green solid line, respectively (Mekuria et al., 2017).

3.3.2 The equilibrum spectra of emitting particles

We have now come up with two basic quantities, the DM density and magnetic field, which are required to calculate the secondary $e^{\pm}$ equilibrium spectra. But we first need to describe the "source spectra" on which the "electrons equilibrium spectra" are based. The "source spectra" is defined as the number of electrons produced per unit time, energy and volume element at the position r from neutralino, χ, annihilation processes and is given by the product of the neutralino pair number density N_{χ}(r), neutralino annihilation rate <σV>, the production spectra $\frac{dN_i^f}{dE}$ and branching ratio B_f, i.e.,

$$Q_i(E,r) =< \sigma V > \sum_f \frac{dN_i^f}{dE} B_f N_{\chi}(r) \tag{3.4}$$

where i and f refer to the produced particle and the allowed annihilation final states each with branching ratio of B_f, respectively. The neutralino pair number density N_{χ}(r) can then be expressed as $\rho_{DM}^2/2m_{\chi}^2$, where the factor 2 in the denominator

appears to take into account the annihilating pairs (Colafrancesco et al., 2006). The production spectra $\frac{dN_i^f}{dE}$ is obtained using DarkSUSY package (Gondolo et al., 2004). The "electrons equilibrium spectra" are then obtained from the "source spectra" of the injected electrons by considering their energy loss by different mechanisms, and their spatial diffusion process as they pass through the atmosphere of the DM halo (Longair, 1994). This process is governed by the diffusion equation in the following form:

$$\frac{\partial}{\partial t}\frac{dn_e}{dE} = \nabla\left(D(E,r)\nabla\frac{dn_e}{dE}\right) + \frac{\partial}{\partial t}\left(b(E,r)\frac{dn_e}{dE}\right) + Q_e(E,r), \tag{3.5}$$

where $\frac{dn_e}{dE}$ is the $e^{\pm}$ equilibrium spectrum, D(E,r) diffusion coefficient, b(E,r) the energy loss factor and Q_e(E,r) the electron "source spectra".

A generic solution to the diffusion equation which in the case of galaxy clusters, where the effect of diffusions of electrons are negligible, is given by Colafrancesco et al. (2006). This solution which is the "electrons equilibrium spectra" has the form:

$$\frac{dn_e}{dE} = \frac{1}{b(E)}\int_{m_e}^{M_\chi} Q_e(E',r)dE', \tag{3.6}$$

where E is the energy of the electrons and b(E) (see Eq. 3.7)is the energy loss term in units of GeV s^{-1} which is the sum of effects due to ICS, synchrotron radiation, Coulomb losses and bremsstrahlung radiation (Colafrancesco et al., 2006).

$$\begin{aligned} b(E) &= b_{IC}E^2(1+z)^4 + b_{sync}E^2B^2 \\ &+ b_{Coul}n_e(1+z)^3\left(1+\frac{1}{75}\log\left(\frac{\gamma}{n_e(1+z)^3}\right)\right) \\ &+ b_{Brem}n_e(1+z)^3\left(\log\left(\frac{\gamma}{n_e(1+z)^3}\right)+0.36\right) \end{aligned} \tag{3.7}$$

Where γ = E/m_e and b_{IC}, b_{synch}, b_{coul}, and b_{brem} are the Inverse Compton Scattering, synchrotron, Coulomb and Bremsstrahlung energy loss factors in units of GeV s^{-1}, respectively. The "electrons equilibrium spectra" can be used to calculate the local emissivities and ultimately the flux, which will be used in the following sections.

3.3.3 Synchrotron emission process

Synchrotron emission is a radiation of a high energy particle gyrating in a magnetic field. It was originally noted in some of the early betatrons where high energy particles were first accelerated to ultrarelativistic energies. This same mechanism is responsible for the radio emission in the galaxy, from supernova reminants and extragalactic radio sources. Diffuse radio emission has been observed in a large number of clusters which is not associated with galaxies (see section 2.2 for more). The distribution of magnetic field, and energetic electrons in the wider region of galaxy clusters is believed to produce synchrotron radiation. For an amplitude of magnetic field B the average power radiated per frequency by electrons with an energy E from synchrotron processes at frequency ν is formulated as in Longair (1994).

$$P_{synch}(\nu, E, r, z) = \int_0^{\pi} d\theta \frac{sin^2\theta}{2} 2\pi\sqrt{3} r_e m_e c \nu_g F_{synch}\left(\frac{\kappa}{sin\theta}\right), \tag{3.8}$$

where m_e is the electron mass, ν_g = $\frac{eB}{2\pi m_e}$ is the non-relativistic gyro-frequency, r_e = $\frac{e^2}{m_e c^2}$ is the classical electron radius, and the dimensionless quantities κ and F_{synch} are defined as

$$\kappa = \frac{2\nu(1+z)}{3\nu_0\gamma^2}\left(1 + \left(\frac{\gamma\nu_p}{\nu(1+z)}\right)^2\right)^{\frac{3}{2}} \tag{3.9}$$

where ν_0 = 2.8 $\times$ 10^{-6} B is the gyro-frequancy and ν_p = 8980 $\times$ 10^{-6} ($(n_{el})^{0.5}$) is the plasma frequancy in units of MHz.

and

$$F_{synch}(x) = x\int_x^{\infty} dy K_{5/3}(y) \simeq 1.25 x^{\frac{1}{3}} e^{-x}(648 + x^2)^{\frac{1}{12}} \tag{3.10}$$

One can obtain the local synchrotron emissivity once the $e^{\pm}$ equilibrium spectra and synchrotron power P_{synch} is determined using the following formula

$$j_{synch}(\nu, r, z) = \int_{m_e}^{M_\chi} dE\left(\frac{dn_{e^-}}{dE} + \frac{dn_{e^+}}{dE}\right) P_{synch}(\nu, E, r, z), \tag{3.11}$$

The quantity $\frac{dn_{e^\pm}}{dE}$ is the $e^{\pm}$ equilibrium spectra obtained after accounting for the energy loss of electron through the atmosphere of the galaxy cluster as the sum

of effects such as ICS, synchrotron emission, Coulomb losses and bremsstrahlung processes. The local synchrotron emissivity at high frequencies, $\nu \gg \nu_c$ will tend to exp(-ν/ν_c) and at low frequencies, $\nu \ll \nu_c$ to $\nu^{1/3}$, where ν_c = $\frac{3}{2}$ γ^2 ν_g sinθ is critical frequency at which we will have the maximum emissivity (Longair, 1994). The flux density within radius r can be expressed as follows:

$$S_{synch}(\nu, z) = \int_0^r d^3r' \frac{j_{synch}(\nu, r', z)}{4\pi D_L^2} \tag{3.12}$$

here the flux density S_{synch}(ν,z) is described in units of Jansky [Jy] and D_L = 96000 kpc is the luminosity distance to the halo.

3.4 The data analysis

The raw data we have taken from the MUSIC simulation contains the DM particle coordinates and masses of two simulated galaxy clusters (i.e, SGC280 and SGC282). From this raw data for the position and mass of DM particle, we used SPH-kernel to determine the density of DM on a grid based on Eq. 3.13 below.

$$\rho_{on\ a\ grid}(r) = \sum_i m_i W(r - r_i, h), \tag{3.13}$$

where $\rho_{on\ a\ grid}$ is the particle density on a grid of size (10 kpc)^3, m_i is the mass of particles (in our case neutralino and gas), the scaling factor W(r$-$r$_i$, h) is called the kernel, and h describes the characterstic width of the kernel which is normilized to unity (Springel, 2010).

Next to this important procedures, we used a fortran code to allocate the DM and gas density on a three dimensional cube of side 2 Mpc which is grided into smaller cubes of side $\sim$ 10 kpc (the simulated galaxy clusters which are (2 Mpc)^3 in volume are divided into $\sim$ 8 millon small cubes of side $\sim$ 10 kpc making 201 grids on each sides of the clusters. Thus, for one side of the clusters the grids give about 40,401 square boxes). Now knowing the DM and gas density in each cube help us to determine and allocate the magnetic field and electron density within the cluster which inturn allow us to compute the gyro- and plasma frequency, respectively according to the relation given under subsection 3.3.3. Combining this results with the electron production spectra from the DarkSUSY package (a fortran package that calculate the yield of particles per a neutralino annihilation and our second data source) enables us to calculate all the necessary ingrediants

for the synchrotron emission i.e, the electron source factor Q_e(E,r), the electron equilibrium spectra $\frac{dn_e}{dE}$ and the average power radiated P(ν,E,r,z) according to the Eqns. 3.4, 3.6 and 3.8, respectively. Finally, the local emissivity and the integrated flux density are computed in each cube based on Eqns. 3.11 and 3.12. In addition to the fortran program we have also used python to produce all our maps.

3.5 Summary

This chapter brought us to the final stage were we have all the quantities that are necessary to accomplish our objectives. We have specified a DM candidate for our work and also have presented all the mathematical models necessary to compute the integrated sychrotron flux from the annihilation process. The data for the two simulated Coma like galaxy clusters (i.e, SGC280 and SGC282) of our interest are found available in the MUSIC-dataset and the DarkSUSY package is our source for the production spectra of a neutralino mass M_χ = 35 GeV. In the next chapter the results and the discussions are presented.

CHAPTER 4

Results and discussion

4.1 Introduction

For the purpose of studying the diffused radio emission from the Coma cluster; DM annihilation/decay processes as the sources of relativistic electrons and the mathematical models discussed in section 3.3 to compute the synchrotron emission have been applied in two simulated Coma like galaxy clusters. Following these, in this chapter, we have presented the results obtained from the study of the diffused radio spectrum of the simulated Coma like galaxy clusters in different forms (i.e, maps, graphs and tables). In the first section the DM distribution and the density maps for the clusters is presented. Then the radio flux and the radio emission maps at different frequencies are discussed. Lastly we have dealt with the integrated radio spectrum and the variation of the spectral index in comparision with other works done by Thierbach et al. (2003) and Giovannini et al. (1993) for the Coma C cluster of galaxies.

4.2 The distribution of the dark matter in the galaxy clusters

The DM density maps shown in Fig. 4.1 are in units of $M_\odot$ kpc^{-3}. They represent the DM distributed in a three dimensional galaxy cluster projected onto a two dimensional map by integrating all the DM density along the line-of-sight. The bright yellow regions on the maps are the densest DM regions in the galaxy clusters. For SGC280 there are two large central structures which are nearly 0.5 Mpc apart but SGC282 have one central dominant structure with other off center substructures which are considerably dense. The maps indicate how the DM density decreases as we go from the center to the edge of the clusters except at the substructures which are found off center. We have observed that SGC282 has quite a number of substructures relative to that of SGC280. It is discussed in section 3.4 that the

cluster sides are grided into a total of 40,401 square boxes, and to observe the DM density variation between the two clusters we take the ratio of DM density contributed from the corresponding boxes of the two clusters. We have found that SGC282 is denser for about 83% of the region, being 155 times denser than SGC280 at its densest point. While SGC280 is denser for the remaining 17% of the region and at its densest point it is only 92 times denser than SGC282. This and other observations of the density maps lead us to the gross generalization that SGC282 is denser than SGC280. Since we have considered equal volume of clusters this result give us the impliction that SGC282 is of high mass.

We have made a comparision of the DM density of this two galaxy clusters

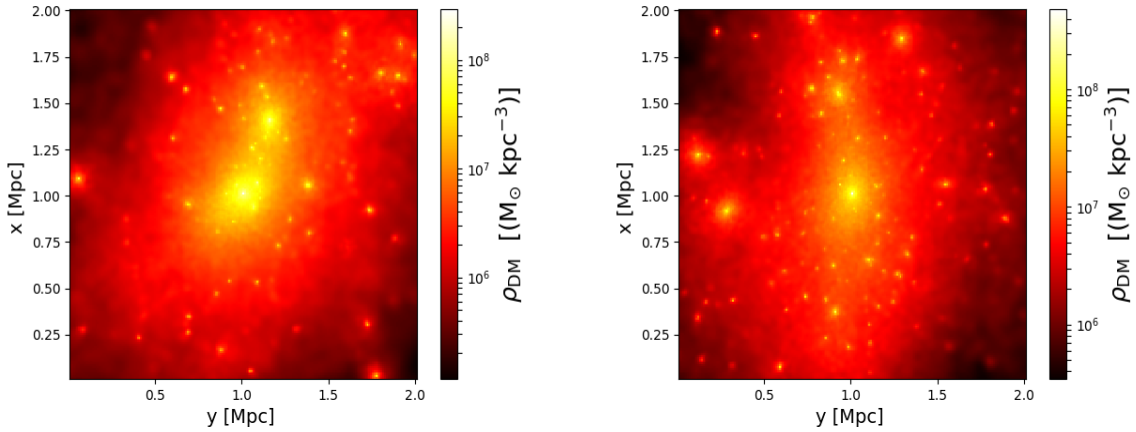

Figure 4.1: The DM density map of SGC280 (left) and SGC282 (right) obtained by integrating the DM density along the line of sight.

by plotting the DM densities binned on log-scale across r as shown in Fig. 4.2. Now the graph clearly indicate us that SGC282 is dense at all radial points than SGC280 supporting the gross generalisation we have made previously. All the uneven features on the curves are due to the contributions from the substructures.

In both the DM denstiy maps and the DM densities binned on log-scale across r, we observe something that will take our attention. For the sake of detecting DM we need to know from which regions of the galaxy cluster are the higher emissions coming from. But we know that the higher emissions originate from the regions of high annihilation rate which is proportional to the square of the DM density (i.e, $\Gamma_{ann} \propto \rho^2_{DM}$). So all the densest regions on the maps which are near the center and off-center are our source (or amplifiers) of higher radio emission. Therefore, the

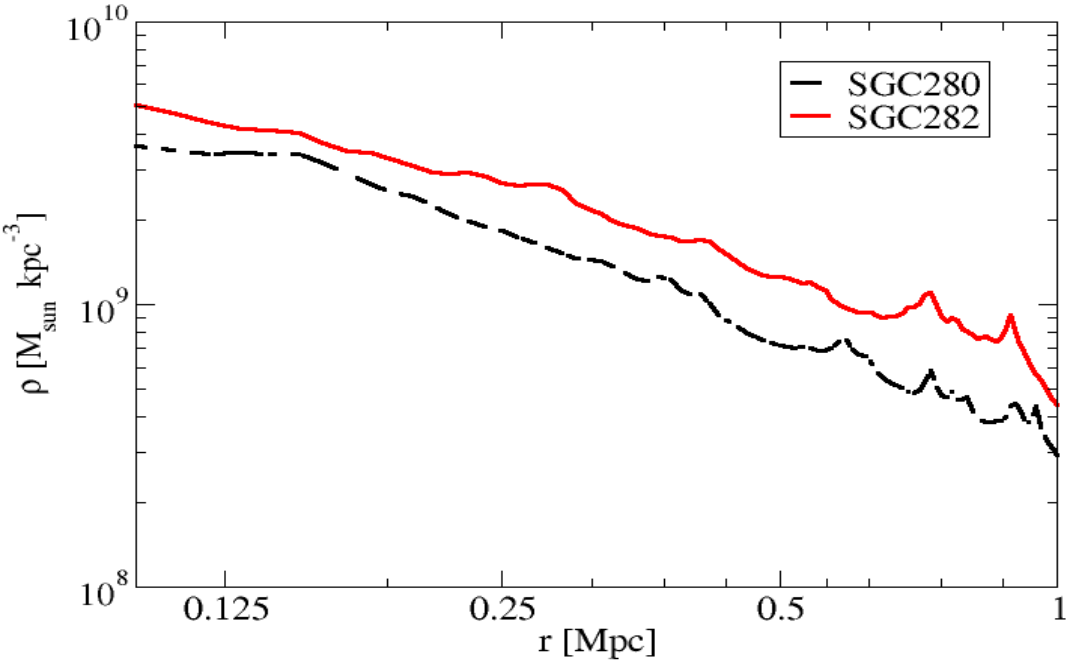

Figure 4.2: Comparision of DM densities binned on log-scale across r from SGC280 and SGC282 indicated in dark broken and red solid curves, respectively.

DM density maps tell us where to expect for the radio emission.

4.3 Radio emission maps and their flux values

Once we have computed the local synchrotron emissivity from Eq. 3.11, the radio flux is calculated according to Eq. 3.12 for a wide range of frequencies. In general, we have observed that the flux values at lower frequencies are much greater than the flux values at higher frequecies and this is due to the fact that the emissivity decays exponentially at higher frequencies. Using the computed flux data from the simulation we are able to produce a good resolution maps that allow us to look for possible structures and substructures distributed in the cluster regions. In Figs. 4.3 and 4.4 the radio flux maps at frequencies 110 MHz and 1.4 GHz of the two galaxy clusters are presented.

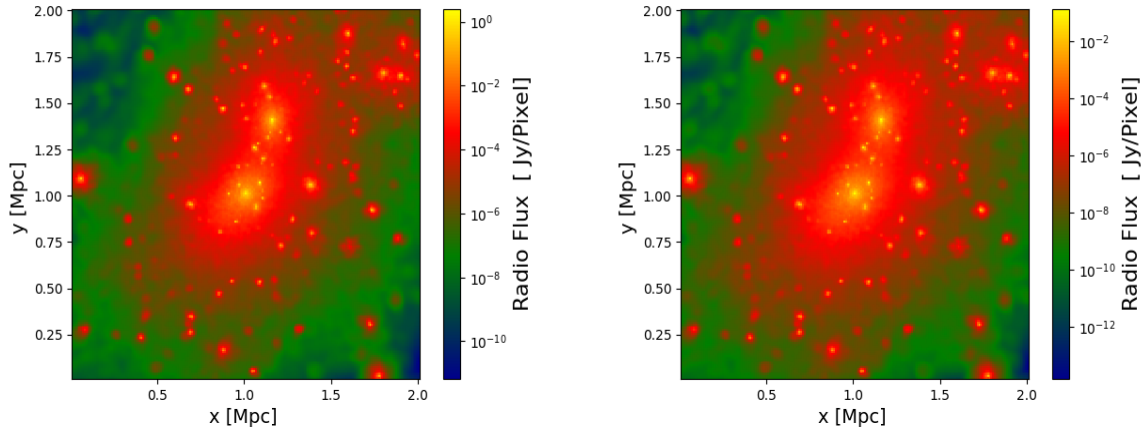

Figure 4.3: Radio emission map of SGC280 at 110 MHz (left) and 1.4 GHz (right), showing no significant morphological difference.

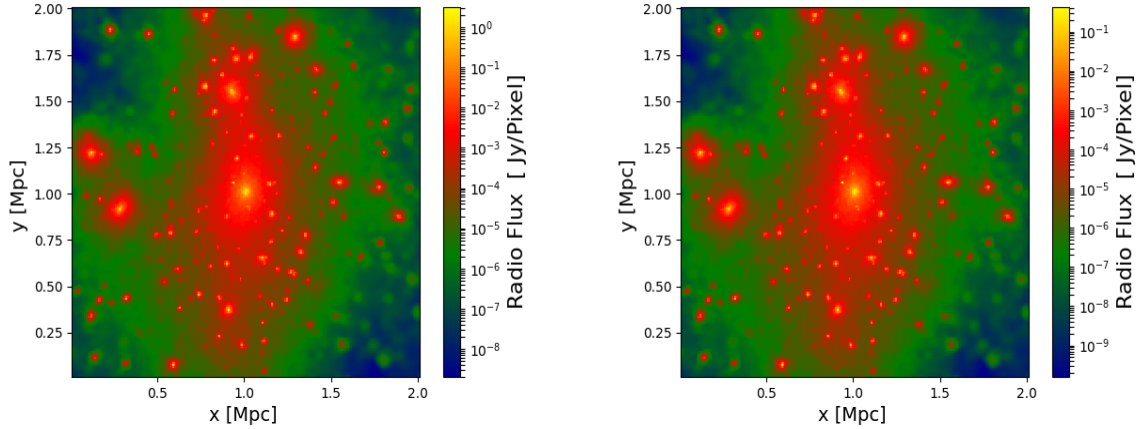

Figure 4.4: Radio emission map of SGC282 at 110 MHz (left) and 1.4 GHz (right) showing no significant morphological difference..

No significant morphological differences are seen between the maps at the two different frequencies, as Giovannini et al. (1993) has reported for the maps of the observed flux of Coma cluster at three different frequencies. Without making a detailed observation one can notice the similarity of this maps with the square density maps in Fig. 3.1, indicating that higher emissions originate from the densest region and lower emissions from the less dense regions as it has been predicted. The central regions and the substructures found off center are also clearly visibile from the maps.

Comparison between maps that are produced at 110 MHz and 1.4 GHz frequencies do not show any noticeable difference on the background structure of the emission apart from the difference in the output flux at the two frequencies. Point-by-point

ratio between flux from the two radio emission maps show flux values at 110 MHz varies between 12 to 433 times that of flux at 1.4 GHz for SGC280 and between 7 to 64 times that of flux at 1.4 GHz for SGC282.

The minimum and maximum flux values and flux densities that we have obtained taking different frequencies are presented in tabular form in Tab. 4.1 below.

In order to make further comparision of the radio flux values at 110 MHz and

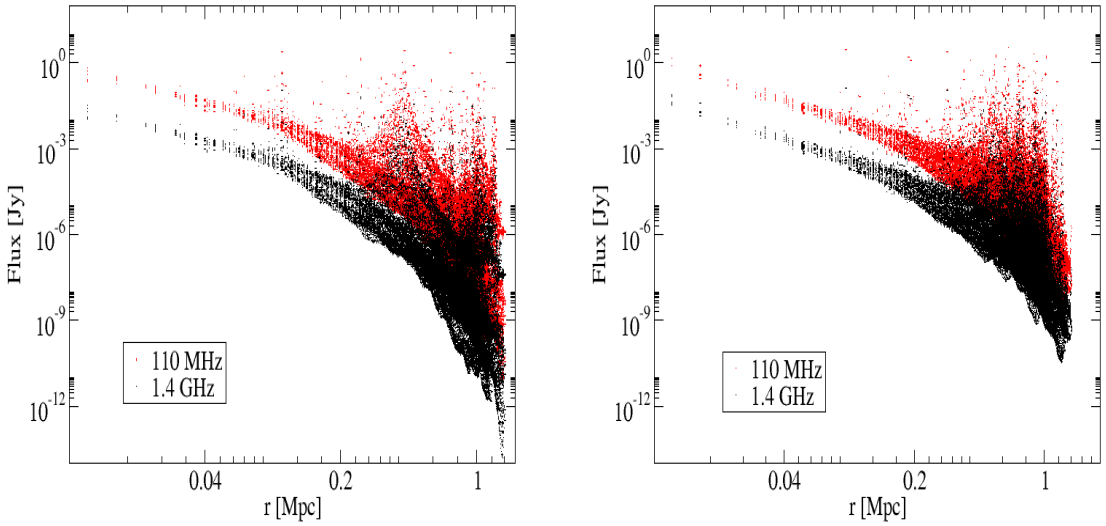

Figure 4.5: The radial distribution of the flux contribution from each boxes at frequencies 110 MHz and 1.4 GHz represented in red and black colors, respectively for SGC280 (left) and SGC282 (right).

1.4 GHz frequencies, we have plotted the flux coming from each boxes against the radial distance of the boxes from the center of the galaxy clusters as shown in Fig. 4.5. In both cases the red colors represent flux at 110 MHz and black colors represent flux at 1.4 GHz. This figures express the difference between the emission maps by showing that for each boxes the radio flux of both clusters at 110 MHz are all higher than the radio flux at 1.4 GHz. And for this reason the red color is seen shifted up. The similarity in the pattern of the profiles and the maps imply the fact that strong radio emissions at any frequency originate from the densest regions of the galaxy clusters with different flux magnitudes.

	GC280			GC282		
Frequency [MHz]	Minimum Flux [Jy]	Maximum Flux [Jy]	Flux density [Jy]	Minimum Flux [Jy]	Maximum Flux [Jy]	Flux density [Jy]
30	4.31×10^{-11}	2.81	48.24	1.08×10^{-8}	3.91	81.75
110	6.58×10^{-12}	o.85	13.95	1.97×10^{-9}	1.09	23.51
300	1.10×10^{-12}	0.28	4.55	4.76×10^{-10}	0.35	7.68
608.5	2.13×10^{-13}	0.12	1.92	1.55×10^{-10}	0.14	3.24
1400	1.52×10^{-14}	0.04	0.66	3.09×10^{-11}	0.05	1.11
4850	2.61×10^{-17}	1.06×10^{-2}	0.12	8.80×10^{-13}	1.23×10^{-2}	0.20
6000	5.63×10^{-18}	6.00×10^{-3}	0.087	3.83×10^{-13}	9.50×10^{-3}	0.15

Table 4.1: Minimum and maximum flux values taking seven different frequencies with their corresponding integrated flux densities.

In addition, we can infere how the flux contribution from each boxes is distributed within the galaxy clusters. For SGC280 the flux contribution from the central large structure goes upto a distance of 0.1 Mpc. In the interval 0.3 - 0.5 Mpc we have the flux contribution of the second large structure and other substructures of the cluster. A significant flux contribution also comes from substructures which are far from the center in the interval 0.8 - 1.2 Mpc. In a similar manner for SGC282 we have flux contribution from the central structure upto a distance of 0.1 Mpc. A significant amount of flux contribution from substructures lies in the interval 0.4 - 1 Mpc where as flux from substructres beyond 1 Mpc is insignificant. We can see that while the minimum flux from the underdense region of SGC280 is the order of 10^{-14} Jy, we have obtained this to be the order of 10^{-11} Jy in SGC282.

4.4 Integrated radio spectrum and spectral index maps

By taking the sum of all the radio flux values at a given frequency we come up with the flux density. Fig. 4.6 is the graph of the flux density versus frequency shown by the curves in red (solid) and dark (broken) colors from our results of SGC282 and SGC280, respectively. In the figure the observational results from Thierbach et al. (2003) for the diffuse radio halo source Coma C galaxy cluster are shown in blue dots for the purpose of comparision. From the curves we can see that the flux density decreases as frequency increases in both cases. This is because of the fact

that particles with high energy (or high frequency) have short radiative life time than the low energetic ones and the emission spectrum is modified accordingly due to the deplation of the high energy particles from the energy distribution (Norris et al., 2013). Our flux density results for SGC280 are in a good agreement with the observational results of Thierbach et al. (2003) for frequencies below $\sim$ 2 GHz but for frequencies greater than $\sim$ 2 GHz it shows a small deviation. The flux densities of SGC282 are above the observed radio spectrum of Coma C cluster almost at all frequencies. The reason is that SGC282 is denser than SGC280 with high annihiation rate and thus higher radio emission.

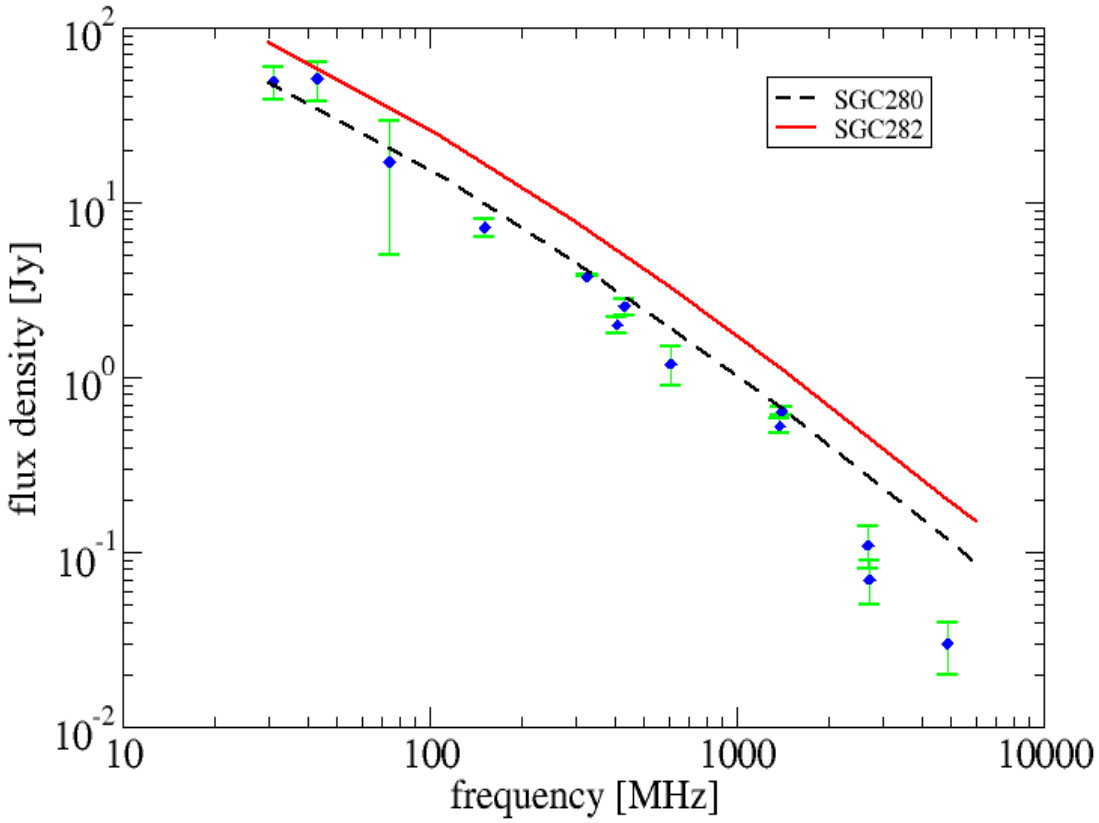

Figure 4.6: Flux density from synchrotron emission of SGC282 and SGC280 indicated in red (solid) and dark (broken) curves, respectively in comparision to the observational data of radio emission of Coma cluster from Thierbach et al. (2003) indicated in blue dots.

The radio flux is characterized by its spectral index (α) value which is given by Eq. 2.1, using this equation we have obtained an average spectral index value of -1.20 for both clusters. The flux density of the two clusters show a power-law dependance which can be described in the form S(α) $\propto \nu^{\alpha}$ = $\nu^{-1.2}$. The average spectral index provides us minimum information which is about the power law dependance of the radio flux. Therefore, we need to see its spatial variation within the cluster regions in order to get a better physical information about the structure of the cluster. In the following two paragraphs we have discussed the spectral index variation and their physical implication in the galaxy clusters.

In section 2.2 we have stated the importance of measuring the spatial distribution of the spectral index. So in Fig. 4.7 we have presented the spectral index map produced from the spatial distribution of spectral index obtained by comparing the flux at 110 MHz and 1.4 GHz frequencies for SGC280 and SGC282, respectively. While the spectral index for SGC280 shows variation in the interval -2.4 at the periphery to -0.98 near the center, for the SGC282 the variation is from -1.63 at the periphery to -0.75 near the center. We have observed a larger steepening of spectral index for SGC280 at the periphery than for SGC282. As we can see from the maps wide region of the cluster shows a spectral flattening with patchy regions due to the small fluctuation of the spectral index in the interval [-1.2, -1.4] and shows high steepening at the clusters edge. It was reported in Giovannini et al. (1993) that the spectral index distribution for the radio spectrum of Coma C shows a centeral region of $\sim$ 170 kpc radius where the spectral index is almost constant ($\sim$ 0.8) (note here that we have used negetive spectral index value), surrounded by a region where the spectrum steepens to α greater than $\sim$ 1.8. Our spectral index values $\sim$ (-0.8, -1.0) and $\sim$ (-1.6, -2.2) obtained in the very center and dark matter substructure (cluster periphery) are in a good agreement with the work of Giovannini et al. (1993).

The difference in the number of high and low energetic electrons at the cluster center and periphery can be seen from the variation of the spectral index. For the clusters periphery where there is spectral steepening, there would be large amount of low energetic electrons than the energetic ones relative to the clusters wider region where there is spectral flattening. The electron energy distribution given by Eq. 2.2 declines to the cluster edge because of the spectral steepening. Since the DM density decreases to the cluster periphery, the annihalation rate of neutralinos

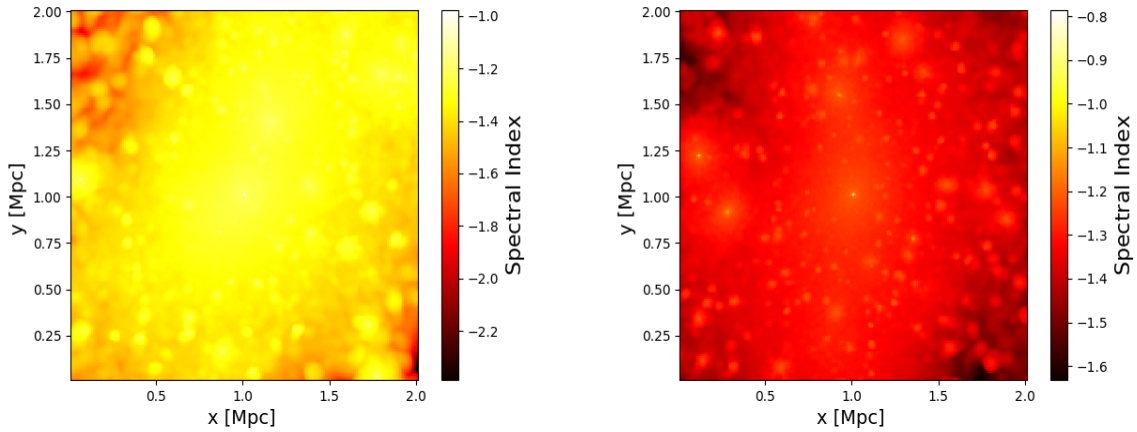

Figure 4.7: The spectral index map of SGC280 (left) and SGC282 (right) produced from the spatial distribution of spectral index values obtained by comparing the fluxes at 110 MHz and 1.4 GHz frequencies.

also decreases giving rise to smaller production of energetic electrons. In addition to this small production of electrons at the cluster periphery the deplation of the created electrons through different loss mechanisms also plays a great role to the large difference in there number and to the spectral steepening. The fact that the magnetic field decreases rapidly at the edge of the cluster (as it can be seen in Fig. 3.2) is associated to the lower radio emission observed at the periphery.

4.5 Summary

In this chapter we have presented the results we have obtained from the DM annihilation of neutralino for the simulated Coma like galaxy clusters using the raw data taken from the MUSIC-dataset. The results enable us to produce a good resolution radio emission maps that allows to look for possible structures and substructures distributed in cluster region which are required to obtain the expected radio emission from DM annihilation process. The radio emission maps and the square of DM density maps were found to be identical proving the fact that higher emission originate from the densest structures. The integrated radio spectrum declines as frequency increases because of the radiative lifetime of the relativistic electrons. The flux density curves have shown that the radio spectrum of SGC280 is in a good agreement with the observed radio spectrum of Coma C cluster of galaxies. The radio spectrum of the two clusters can be described in a power-law form with the same average spectral index value of -1.2. The spatial

variation of the spectral index has been observed to be flat for a wider region of the cluster with small fluctuation resulting in patchy regions on the maps.

CHAPTER 5
Conclusion

DM is the dominant component of galaxies and clusters of galaxies. It plays a great role in the formation and morphological evolution of these huge gravitationally bounded systems. Nevertheless, its true nature is still elusive. We have investigated DM indirectly by studying the non-thermal radio emission from their annihilation processes in simulated Coma like galaxy clusters. We computed the radio emission from the neutralino DM annihilation considering a neutralino mass of M_{χ} = 35 GeV, in two simulated Coma like galaxy clusters whose raw datas for the particle mass and coordinate are taken from the MUSIC-dataset. Using the flux results we are able to produce a good resolution maps of the radio emission that allow us to look for possible structures and substructures distributed in the cluster regions. No significant morphological differences were observed between the maps at different frequencies and the radio emission maps are found to be identical to the DM density maps indicating that higher emissions originate from the densest regions. The radio emissions at lower frequencies are observed to be higher as compared to emissions at high frequencies.

Our result for the integrated radio spectrum of SGC280 is in a good agreement with the observed radio spectrum of the Coma cluster of galaxies at frequecies below $\sim$ 2 GHz but it shows small deviation for frequencies above $\sim$ 2 GHz. While the radio spectrum obtained for SGC282 is high almost for all the frequencies corresponding to the fact that it is denser than SGC280. It can be said that the SGC280 is a good representative of the dark matter distribution in the Coma cluster of galaxies. For both clusters the spectral index have shown flattenig for wider region of the cluster with a small fluctuation showing patchy regions on the map and steepening at the cluster periphery.

Since galaxy clusters are dominated by DM, it is appropriate to consider the third model (i.e, Secondary electrons from DM annihilation/decay processes) as the source

of the relativistic electrons which are responsible for the diffuse radio emission in galaxy clusters. But ignoring all the other models is not effective; because merging clusters that give rise to violent turbulence and shock waves as suggested by the Primary electron model, and hadronization processes (i.e, pp collisions) in the Secondary electron model are quite common phenomenas in clusters. So we have planned to extend this work: 1. using different annihilation channels and masses of neutralino to come up with the best fit to the observed radio spectrum of Coma cluster and 2. considering a new model that will give a consideration to all the suggested models according to their significance.

Bibliography

George O Abell, Harold G Corwin Jr, and Ronald P Olowin. A catalog of rich clusters of galaxies. *The Astrophysical Journal Supplement Series*, 70:1–138, 1989.

Peter AR Ade, N Aghanim, M Arnaud, M Ashdown, J Aumont, C Baccigalupi, AJ Banday, RB Barreiro, JG Bartlett, N Bartolo, et al. Planck 2015 results-xiii. cosmological parameters. *Astronomy & Astrophysics*, 594:A13, 2016.

Ch Alcock, Carl W Akerlof, RA Allsman, TS Axelrod, DP Bennett, S Chan, KH Cook, KC Freeman, K Griest, SL Marshall, et al. Possible gravitational microlensing of a star in the large magellanic cloud. *Nature*, 365(6447):621, 1993.

E Aliu, S Andringa, S Aoki, J Argyriades, K Asakura, R Ashie, H Berns, H Bhang, A Blondel, S Borghi, et al. Evidence for muon neutrino oscillation in an accelerator-based experiment. *Physical review letters*, 94(8):081802, 2005.

Baidyanath Basu, TANUKA CHATTOPADHYAY, and SUDHINDRA NATH BISWAS. *An introduction to Astrophysics*. PHI Learning Pvt. Ltd., 2010.

Gianfrance Bertone, D Hooper, and J Silk. Particle dark matter: Evidence, candidates and constraints, phys. rept. 405 (2005) 279–390. *arXiv preprint hep-ph/0404175*, 5.

A Bonafede, L Feretti, M Murgia, F Govoni, G Giovannini, D Dallacasa, K Dolag, and GB Taylor. The coma cluster magnetic field from faraday rotation measures. *Astronomy & Astrophysics*, 513:A30, 2010.

G Brunetti, G Setti, L Feretti, and G Giovannini. Particle reacceleration in the coma cluster: radio properties and hard x-ray emission. *Monthly Notices of the Royal Astronomical Society*, 320(3):365–378, 2001.

S Colafrancesco, P Marchegiani, and G Beck. Evolution of dark matter halos and their radio emissions. *Journal of Cosmology and Astroparticle Physics*, 2015(02): 032, 2015.

Sergio Colafrancesco and Barbara Melé. Neutralinos and the origin of radio halos in clusters of galaxies. *The Astrophysical Journal*, 562(1):24, 2001.

Sergio Colafrancesco, Stefano Profumo, and Piero Ullio. Multi-frequency analysis of neutralino dark matter annihilations in the coma cluster. *Astronomy & Astrophysics*, 455(1):21–43, 2006.

Peter Coles and Francesco Lucchin. *Cosmology: The origin and evolution of cosmic structure*. John Wiley & Sons, 2003.

Carlo R Contaldi, Henk Hoekstra, and Antony Lewis. Joint cmb and weak lensing analysis; physically motivated constraints on cosmological parameters. *arXiv preprint astro-ph/0302435*, 2003.

Alan Dressler. Galaxy morphology in rich clusters-implications for the formation and evolution of galaxies. *The Astrophysical Journal*, 236:351–365, 1980.

K Eguchi et al. First results from kamland: Evidence for reactor anti-neutrino disappearance, 2003. *Phys. Rev. Lett*, 90:021802.

L Feretti and G Giovannini. A pan-chromatic view of clusters of galaxies and the large-scale structure, ed. m. plionis, o. lopez-cruz, & d. hughes. *Lecture Notes in Physics*, 740:143, 2008.

Luigina Feretti, E Orru, G Brunetti, G Giovannini, N Kassim, and G Setti. Spectral index maps of the radio halos in abell 665 and abell 2163. *Astronomy & Astrophysics*, 423(1):111–119, 2004.

Luigina Feretti, Gabriele Giovannini, Federica Govoni, and Matteo Murgia. Clusters of galaxies: observational properties of the diffuse radio emission. *The Astronomy and Astrophysics Review*, 20(1):54, 2012.

C Ferrari, F Govoni, S Schindler, AM Bykov, and Y Rephaeli. Observations of extended radio emission in clusters. In *Clusters of Galaxies*, pages 93–118. Springer, 2008.

G Giovannini, L Feretti, T Venturi, K-T Kim, and PP Kronberg. The halo radio source coma c and the origin of halo sources. *The Astrophysical Journal*, 406: 399–406, 1993.

Paolo Gondolo, Joakim Edsjö, Piero Ullio, Lars Bergström, Mia Schelke, and Edward A Baltz. Darksusy: Computing supersymmetric dark matter properties numerically. *Journal of Cosmology and Astroparticle Physics*, 2004(07):008, 2004.

John F Hawley and Katherine A Holcomb. *Foundations of modern cosmology*. Oxford University Press, 2005.

Marco Hernandez, Tian Ma, and Shouhong Wang. Theory of dark energy and dark matter. *J. Math. Study*, 48(3):199–221, 2015.

N Jarosik, CL Bennett, J Dunkley, B Gold, MR Greason, M Halpern, RS Hill, G Hinshaw, A Kogut, Eiichiro Komatsu, et al. Seven-year wilkinson microwave anisotropy probe (wmap*) observations: sky maps, systematic errors, and basic results. *The Astrophysical Journal Supplement Series*, 192(2):14, 2011.

Gerard Jungman, Marc Kamionkowski, and Kim Griest. Supersymmetric dark matter. *Physics Reports*, 267(5-6):195–373, 1996.

Nick Kaiser and Gordon Squires. Mapping the dark matter with weak gravitational lensing. *The Astrophysical Journal*, 404:441–450, 1993.

SM Kent and JE Gunn. The dynamics of rich clusters of galaxies. i-the coma cluster. *The Astronomical Journal*, 87:945–971, 1982.

Michael Klasen, Martin Pohl, and Günter Sigl. Indirect and direct search for dark matter. *Progress in Particle and Nuclear Physics*, 85:1–32, 2015.

Anatoly A Klypin, Sebastian Trujillo-Gomez, and Joel Primack. Dark matter halos in the standard cosmological model: Results from the bolshoi simulation. *The Astrophysical Journal*, 740(2):102, 2011.

Edward W Kolb and Michael S Turner. The early universe (redwood city, 1990.

MI Large, DS Mathewson, and CGT Haslam. A high-resolution survey of the coma cluster of galaxies at 408 mc./s. *Nature*, 183(4676):1663, 1959.

Mariangela Lisanti. Lectures on dark matter physics. In *TASI 2015: New Frontiers in Fields and Strings*, pages 399–446. World Scientific, 2017.

Malcolm S Longair. *High energy astrophysics*. cambridge university Press, 2011.

MS Longair. High energy astrophysics, volume 2, stars, the galaxy and the interstellar medium, ed. ms longair, 1994.

Vladimir Luković, Paolo Cabella, and Nicola Vittorio. Dark matter in cosmology. *International Journal of Modern Physics A*, 29(19):1443001, 2014.

Maxim Markevitch, F Govoni, G Brunetti, and D Jerius. Bow shock and radio halo in the merging cluster a520. *The Astrophysical Journal*, 627(2):733, 2005.

Remudin Reshid Mekuria, Paolo Marchegiani, Andreas Faltenbacher, and Sergio Colafrancesco. Multi-wavelength emissions from dark matter annihilation processes in galaxy clusters using cosmological simulations. *PoS*, page 009, 2017.

R Benton Metcalf and Piero Madau. Compound gravitational lensing as a probe of dark matter substructure within galaxy halos. *The Astrophysical Journal*, 563 (1):9, 2001.

Ray P Norris, J Afonso, David Bacon, Rainer Beck, Martin Bell, RJ Beswick, Philip Best, Sanjay Bhatnagar, Annalisa Bonafede, Gianfranco Brunetti, et al. Radio continuum surveys with square kilometre array pathfinders. *Publications of the Astronomical Society of Australia*, 30, 2013.

Jan H Oort. The force exerted by the stellar system in the direction perpendicular to the galactic plane and some related problems. *Bulletin of the Astronomical Institutes of the Netherlands*, 6:249, 1932.

Miguel A Perez-Torres, Fabio Zandanel, Martin A Guerrero, Sabyasachi Pal, Stefano Profumo, Francisco Prada, and Francesca Panessa. The origin of the diffuse non-thermal x-ray and radio emission in the ophiuchus cluster of galaxies. *Monthly Notices of the Royal Astronomical Society*, 396(4):2237–2248, 2009.

Aldo Rodríguez-Puebla, Peter Behroozi, Joel Primack, Anatoly Klypin, Christoph Lee, and Doug Hellinger. Halo and subhalo demographics with planck cosmological parameters: Bolshoi–planck and multidark–planck simulations. *Monthly Notices of the Royal Astronomical Society*, 462(1):893–916, 2016.

Kurt Roettiger, Jack O Burns, and James M Stone. A cluster merger and the origin of the extended radio emission in abell 3667. *The Astrophysical Journal*, 518(2): 603, 1999.

Matts Roos. *Introduction to cosmology*. John Wiley & Sons, 2015.

Vera Rubin. Dark matter in the universe. *Scientific American*, 1:106–110, 1998.

Stéphanie Ruphy. Limits to modeling: Balancing ambition and outcome in astrophysics and cosmology. *Simulation & Gaming*, 42(2):177–194, 2011.

Dongsu Ryu, Hyesung Kang, Eric Hallman, and TW Jones. Cosmological shock waves and their role in the large-scale structure of the universe. *The Astrophysical Journal*, 593(2):599, 2003.

Dennis William Sciama. *Modern cosmology and the dark matter problem*. Number 3. Cambridge University Press, 1993.

Federico Sembolini, Gustavo Yepes, Marco De Petris, Stefan Gottlöber, Luca Lamagna, and Barbara Comis. The music of galaxy clusters–i. baryon properties and scaling relations of the thermal sunyaev–zel'dovich effect. *Monthly Notices of the Royal Astronomical Society*, 429(1):323–343, 2012.

Raymond A Serway, Clement J Moses, and Curt A Moyer. *Modern physics*. Cengage Learning, 2004.

Volker Springel. The cosmological simulation code gadget-2. *Monthly notices of the royal astronomical society*, 364(4):1105–1134, 2005.

Volker Springel. Smoothed particle hydrodynamics in astrophysics. *Annual Review of Astronomy and Astrophysics*, 48:391–430, 2010.

M Thierbach, U Klein, and R Wielebinski. The diffuse radio emission from the coma cluster at 2.675 ghz and 4.85 ghz. *Astronomy & Astrophysics*, 397(1):53–61, 2003.

V Vacca, L Feretti, G Giovannini, F Govoni, M Murgia, RA Perley, and TE Clarke. Spectral index image of the radio halo in the cluster abell 520, which hosts the famous bow shock. *Astronomy & Astrophysics*, 561:A52, 2014.

F Vazza, M Brüggen, R van Weeren, A Bonafede, K Dolag, and G Brunetti. Why are central radio relics so rare? *Monthly Notices of the Royal Astronomical Society*, 421(3):1868–1873, 2012.

Christian Weinheimer. The neutrino mass direct measurements. *arXiv preprint hep-ex/0306057*, 2003.

PN Wilkinson, DR Henstock, IWA Browne, AG Polatidis, P Augusto, ACS Readhead, TJ Pearson, W Xu, GB Taylor, and RC Vermeulen. Limits on the cosmological abundance of supermassive compact objects from a search for multiple imaging in compact radio sources. *Physical Review Letters*, 86(4):584, 2001.

DECLARATION

ADDIS ABABA UNIVERSITY
COLLEGE OF NATURAL AND COMPUTATIONAL SCIENCES
DEPARTMENT OF PHYSICS

MSc Thesis

Non-Thermal Radio Emission from Dark Matter Annihilation Processes in Simulated Coma like Galaxy Clusters

Name of Candidate: Fitsum W/Gerima Beyene

I the under signed declare that the thesis is my original work and no part of it can be claimed as an intellectual property of anybody else except me and my advisors.

Signature: _____